SULEWSKI, LEANNE, M.A. Spectral and Spatial Semi-Automated Detection of Thermokarst Change in the Alaskan Arctic. (2010)
Directed by Roy S. Stine, PhD. 106 pp.

The Arctic is considered the most susceptible environment to climate change, and as such has been of particular interest to climate change researchers. One such effect of climate change in the arctic is the increased incidence of thermokarst activity. Remote sensing technologies have been utilized to help detect thermokarst activity in the region, though typically thermokarst studies are multi-temporal analyses requiring multiple images and considerable time.

This research sought to create a program that could detect thermokarst change from two images of different time periods. 1978 false color infrared aerial photographs, a 2005 SPOT image, and two Landsat images (2002 and 2006) encompassing the 20 kilometer radius around the Toolik Lake Field Station, Alaska, were utilized for this research. Spectral ranges were determined for each image and used as the criteria to numerically classify the two image pixels as water (1), thermokarst (3), and water (6). These images were then subtracted from each other to yield a numerical output containing information on the type of change, if any, that occurred on the landscape. These steps were compiled into one model for each possible change detection using Spatial Modeling Language (SML), and scripts were generated. ERDAS Macro Language (EML) was then used to create the graphical user interface that would allow the models

to run based on user-input of before and after images and the creation of an output image.

Program trials on three watersheds with known thermokarst activity and three without known thermokarst activity indicate that the program achieved its objective of identifying thermokarst activity, with an overall accuracy of 52%. The program was also able to identify areas that did not have any thermokarst activity, with an accuracy of 93.8%. The program did, however, identify lake perimeters as water change, whether as an increase or a decrease.

SPECTRAL AND SPATIAL SEMI-AUTOMATED DETECTION OF THERMOKARST CHANGE IN THE ALASKAN ARCTIC

by

Leanne Sulewski

A Thesis Submitted to
the Faculty of The Graduate School at
The University of North Carolina at Greensboro
in Partial Fulfillment
of the Requirements for the Degree
Master of Arts

Greensboro
2010

Approved by

Roy S. Stine, PhD.
Committee Chair

This thesis is dedicated to my Grandfather, Edward Grabowski, who always supported me and gave me moral encouragement, whether near or far. And, to my parents, Claire and Anthony Sulewski, who always supported me morally and financially (and humored me).

APPROVAL PAGE

This thesis has been approved by the following committee of the Faculty of the Graduate School at the University of North Carolina at Greensboro.

Committee Chair Roy S. Stine, PhD.

Committee Members P. Dan Royall, PhD.

Zhi-Jun Liu, PhD.

_____

Date of Acceptance by Committee

_____

Date of Final Oral Examination

ACKNOWLEDGEMENTS

I would like to acknowledge my committee chair, Dr. Roy Stine, for his guidance and support, whether in Alaska or at UNCG, through this whole process. Without his expertise, this project would not have been possible. I would also like to acknowledge my other committee members, Dr. P. Dan Royall and Dr. Z.J. Liu, for their guidance throughout the writing and editing processes.

I would also like to acknowledge Dr. Prasad Pathak, who, whether it was in the lab or over chat, was always willing to offer moral and technical support. A big "thank you" to Mary "Beebe" Hall-Brown, who always shared my enthusiasm, no matter how little the accomplishment! I would also like to extend my sincere gratitude Dr. Mayur Gosai, who also offered moral and technical support, despite his busy schedule. Also many thanks to my friends who offered moral support: Sunny Chudgar, Lauren Phillips, Katherine Wilson, and Evan Rosegren.

This research was also a part of a National Science Foundation funded grant (0516043).

TABLE OF CONTENTS

Page

LIST OF TABLES

Page

LIST OF FIGURES

Page

CHAPTER I

INTRODUCTION

Natural phenomena are often extremely complex, with many intricate facets interacting in their creation. Thermokarst is one such phenomenon. Thermokarst, loosely defined, is the thawing and collapse of permafrost in the Arctic environments. It manifests itself in numerous different ways and is associated with the larger phenomenon of climate change. Its association with climate change makes it of particular interest to researchers, and remote sensing and Geographic Information Science (GIS) are powerful tools to help these researchers locate and quantify thermokarst activity

1.1. Study Area

1.1.1. Upper Kuparuk River Region

The major area of interest for this research is the Upper Kuparuk River Region located in the Alaskan Arctic, between the central and eastern Brooks Range, near the Toolik Lake Field Station (Figure 1.1). Though the central Brooks Range is tectonically stable, the eastern portion has maintained activity through the Quaternary period. This

region has been subject to many processes that have produced a complex glacial geology unique to the region. These factors work collectively to generate this landscape, including tectonic activity in the northern edge of the Brooks Range, multiple "source areas" for glaciers, and recurring glacial advances (Hamilton, 2001).

Figure 1.1. Toolik Lake Field Station, AK, reference map.

This area has undergone four glaciations: Gunsight Mountain, Anaktuvuk River, Sagavanirktok River, and Itkillik. The Gunsight Moutain (late Tertiary period) and Anaktuvuk River (early Pleistocene epoch) are the two oldest advances. The next of the glaciations, the Sagavanirktok River, dates from 780,000 to 125,000 years before present (middle of the Quaternary period). Finally, the Itkillik glaciation, subdivided into the Itkillik I and Itkillik II advances, is the youngest of the four, occurring after the Sagavanirktok River glaciation in the Pleistocene epoch (Hamilton, 2001).

Adding further complexity to the already multifarious glacial geology of the region is the presence of permafrost. Though the thickness of the permafrost is unknown, it is estimated to be 150 to 250 meters deep, and the active layer ranges from 0.25 to 0.3 meters deep. The existence of permafrost in the region also promotes solifluction. Solifluction is the movement of soil during the seasonal thaw of the active layer. The existence of permafrost in the region also makes it a prime location to study the incidence of thermokarst. In addition to thermokarst, the Upper Kuparuk River Region has a plethora of other periglacial landforms, including but not limited to non-sorted circles, ice-wedge polygons, and palsas (Hamilton, 2001; Balser and Walker, 2003).

This glacial geology also helps to define the vegetation in the area. Vegetation patterns are related to numerous factors including topography and landscape age. Landscape age is closely associated with biomass, as older landscapes tend to have large

amounts of biomass (Walker et al., 1994). These factors become increasingly important when classifying vegetation in this region.

1.1.2. Toolik Area

The research area is within 20 kilometers of the Toolik Lake Research Station (Figure 1.2). It is located within the upper Kuparuk River Region at 68 º 38' N latitude and 149 º 26' W longitude in the foothills of the Brooks Range. Toolik Lake itself was not formed until after the glaciations. The eastern shore of Toolik Lake is a meltwater outlet formed during the Itkillik II advance, which continues northeast into a narrow channel. The lake likely formed by the melting of a stagnant glacier (Hamilton, 2001).

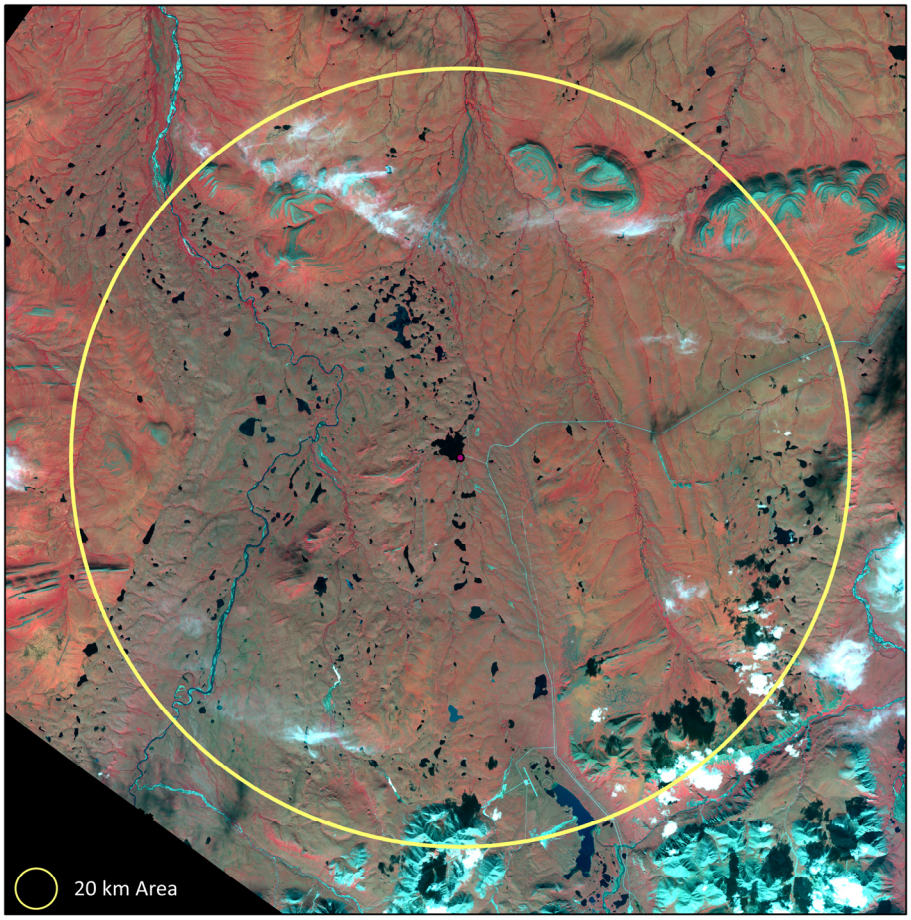

Figure 1.2. 20 km radius around Toolik Lake Field Station.

1.2. Statement of Problem

Much of the research on climate change in the Arctic is in preliminary stages, especially with regards to remote sensing. Firstly, there is still no agreed upon classification scheme for Arctic land cover. Without a standard classification scheme, effective change detection for the Arctic region cannot be performed to assess the potential impacts of climate change (Walker et al., 2002; Stow et al., 2004). Though there is currently no standard classification, one such classification is currently being

formulated for the Trans-Arctic region called “Circumpolar Arctic Vegetation Map” (Walker et al., 2002). The creation of such a scheme would aid in the location of thermokarst activity. The study of thermokarst landform changes in the Arctic is also of increasing importance to climate change scientists. There is a need to quickly locate thermokarst landforms, especially to further study them and their relation to climate change.

1.3. Rationale and Significance

1.3.1. Significance of Arctic Climate Change

Climate change has been an issue of importance to the scientific community for several decades, and it continues to be at the forefront of many scientific research projects. Climate change is an especially important phenomenon in the Arctic, which is considered to be the most susceptible environment to its effects. Its susceptibility is due to its ability to respond to temperature dynamics in a short time period and a plethora of interlinked variables leading to a positive feedback cycle that perpetuates the potential effects of climate change (Overpeck et al., 1997; Serreze et al., 2000; Chapin III et al., 2005; Jia & Epstein 2003; Hinzman et al. 2005). Additionally, the Arctic is one of the least disturbed biomes on the Earth, which makes it an ideal location for noticing the changes due to climate change (Overpeck et al., 1997; Hinzman et al., 2005). Knowledge of climate change in the Arctic may help researchers to further

understand global climate change and its effects not just in this environment, but on a broader scale.

1.3.2. Significance of Thermokarst

The incidence of thermokarst is increasing in response to global climate change, and it can have many significant effects on the surrounding environment. It is considered as one of the major problems facing the northern Arctic regions as a result of warming (Osterkamp et al., 2000). Formation of thermokarst indicates that an ecosystem is going through major alterations (Toniolo et al., 2008). It can also completely destroy or convert areas to other ecosystems (Romanovsky et al., n.d.). The increased incidence of thermokarst may also increase the area of wetlands and ponds which can amount to increases in methane emissions. Studies have shown that lake expansion from 1974 to 2000 has increased methane emissions by 58 percent in North Siberian lakes (Serreze et al., 2000; Walter et al., 2006).

1.4. Research Goals

This research seeks to develop methods and a program that will rapidly identify areas of potential thermokarst activity so further examination of these sites may be conducted. In doing so, this research aims to provide a better understanding of how remote sensing and geographic information science (GIS) can be used to identify areas of thermokarst activity and quantify the changes caused by thermokarst activity.

1.5. Thesis structure

This thesis will be separated into five chapters. Chapter one will be a brief overview of the study area, research questions, and significance. Chapter two will provide an overview of the relevant literature on thermokarst and the Arctic environment's changes due to climate change. Chapter three includes a description of the remote sensing and GIS methods used in this research. Chapter four will provide the results and discussions of the research. Finally, chapter five will discuss the conclusions and implications of this research.

CHAPTER II

LITERATURE REVIEW

2.1. Climate Change Trends in the Arctic

The Arctic is considered the environment most susceptible to climate change, especially considering the positive feedback mechanisms operating in the Arctic, which serve to amplify its effects (Chapin et al. 2005; Overpeck et al. 1997; Jorgenson et al. 2008). Snow and ice cover, with their high albedo and low thermal conductivity, have major influence on these positive feedbacks. For example, as the snow and ice melt, there is less cover to reflect energy back, which further increases energy absorption and melting and so forth (Solomon et al. 2007; ACIA 2004; Serreze et al. 2000).

The Arctic has had twice the amount of mean warming than the global mean, with recent Arctic summers being the warmest in the last 400 years (Rinke and Dethloff 2008; Serreze et al. 2000; Overpeck et al. 1997). Warmer temperatures have a number of implications for the Arctic ecosystems. For example, these warmer temperatures will provide a longer growing season for plants. Warmer temperatures also facilitate the growth of denser, taller forest cover, which will lead to the migration northward of the

treeline and the already documented expansion on shrubs (Chapin et al. 2005; Jia and Epstein 2003; Stow et al. 2004; ACIA 2004; Sturm et al. 2001). Warmer temperatures, and the projected increase in winter precipitation, will additionally lead to earlier melting of the snow cover, especially in the spring and summer months. Another effect of warmer temperatures is the decline in ice extent and warming of permafrost. These warmer temperatures in the Arctic are likely to have implications not only at the regional scale, but at the global scale as well. The documented and continued melting of glaciers, ice caps, and ice sheets are all contributors to global sea level rise (Hinzman et al. 2005; ACIA 2004; Serreze et al. 2000). Additionally, melting of such cyrospheric entities can lead to a reduction and the eventual break down of the thermohaline circulation, which draws heat from the tropics to the northerly latitudes. Since the 1980s, atmospheric warming has also led to the temperature of the top of permafrost has increased an average of 3ºC. This warming of permafrost can lead to the collapses in the permafrost, termed thermokarst (ACIA 2004; Stow et al. 2004; Goldman, 2002; Jorgenson et al. 2001; Sturm et al., 2001; Serreze et al., 2000; Ainsimov & Nelson, 1996; Romanovsky et al., n.d.).

2.2. Thermokarst

Though similar in name to its cousin "karst," thermokarst has many fundamental differences from limestone karst. Limestone karst forms through chemical weathering processes, while thermokarst is more of a mechanical phenomenon, resulting from

freeze-thaw processes. Thermokarst, or “aaaa” as it is termed in Russian, manifests itself in a variety of forms on the landscape (Burn 1992). The manifestations of this phenomenon are potential indicators of climate change, thus understanding and locating them are of importance to both Arctic and climate change researchers.

2.2.1. Geomorphology of Thermokarst

The term thermokarst was coined in 1932 by M.M. Emoaleav and has come to refer landforms that are created by the subsidence of land from the thawing of underlying permafrost (Kodial et al. 2005; Murton 2001; Murton 1996; Burn 1992; Embleton and King 1975). While the stages outlined are different, Arctic researchers agree that thermokarst is part of an “endogenous” cycle (Kirpotin et al. 2009; Murton 2009). The five major stages are:

1. Initiation,
2. Increases in size,
3. Drainage,
4. Stabilization,
5. And recovery (Figure 2.1).

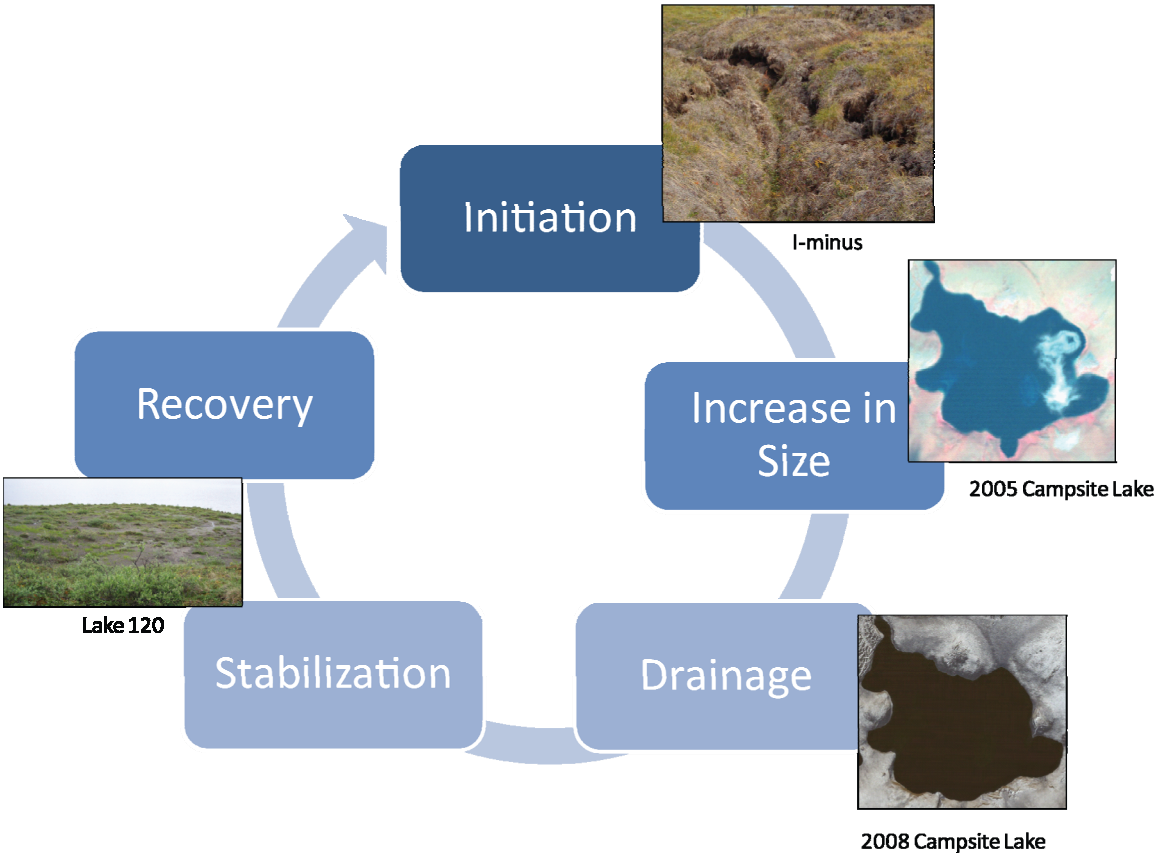

Figure 2.1. Thermokarst cycle (I-minus photo credit: Mary Hall-Brown; Lake 120 photo credit: Prasad A. Pathak).

First, initiation occurs where the ground temperature increases enough to thaw the underlying ice, which may cause ground subsidence. There are several processes that can initiate thermokarst, including but not limited to active-layer deepening, ice-wedge melting, thaw slumping, and groundwater flow. These processes may act alone or interact in the initiation process, which makes understanding thermokarst and its origins complex (Murton 2009). After initiation, the thermokarst will increase in size, and as

the permafrost further degrades, it may lead to lake drainage of its water (Smith et al. 2005). These stages are followed by stabilization, where the activity ceases when some equilibrium has been restored. The final stage, recovery, occurs when permafrost re-aggrades and that may take millennia if it occurs. The time scales for the totality of the thermokarst cycle may vary from decades to centuries to millennia (Murton 2009; Osterkamp et al. 2000). Often times with this thermokarst cycle comes changes in vegetation. Thermokarst can alter moisture conditions, where the karst may accumulate moisture and have the water table nearer to the surface, where areas further away may become drier. Following thermokarst activity, there may be increases in vascular plants such as sedges and deciduous and evergreen shrubs (Schuur et al. 2007). Of particular interest in this research are the stages of initiation, increase in size, and drainage.

Just as the time scales vary, so do the landforms that are considered to be thermokarst, and they are formed in a variety of ways. There are considered to be 22 different thermokarst landforms that are initiated by permafrost degradation (Jorgenson et al. 2008). Each of these landforms varies between and within their individual classifications. For example, thermokarst lakes can contain both shallow and deeps zones, and be formed from many different types of sediment, such as alluvial, colluvial, and lacustrine (Murton 2001; Murton 1996). Also, the location of thermokarst makes a difference in how it manifests. For example, thermokarst formed in

discontinuous permafrost tends to result in a decrease in lake area, while those formed in continuous permafrost tend to result in an increase in lake area (Kirpotin et al. 2009). Even with all of these differences, all thermokarst have two important geomorphic consequences in common: thermokarst reduces soil strength and reduces soil volume (Murton 2009).

2.2.2. Thermokarst and Climate Change

The Arctic is considered the most susceptible environment to climate change, and climate change is one of many factors that can initiate thermokarst activity (Murton 2009). The observed increase in permafrost temperatures in the Arctic over the last 20 or 30 years, including Alaska, has already begun to increase the incidence of thermokarst (Osterkamp 2005; Romanovsky et al. n.d.). Though climate change can initiate thermokarst, these findings must be viewed with caution, because thermokarst is not only initiated by climate change (Murton 2009; Harris 2002).

In addition to being initiated by climate change, thermokarst also serves to enhance climate change. Methane and Carbon Dioxide, two greenhouse gases, are released by thermokarst activity (Walter et al. 2006; Hinkel et al. 2005; Osterkamp et al. 2000). Of particular concern is methane, for it has a greater global warming potential than even Carbon Dioxide. Walter et al. (2006) found that thawing permafrost accounted for most of the methane emissions from lakes in Siberia. It was also found

that the expansion of these Siberian lakes due to thermokarst activity between 1974 and 2000 accounted for an increase in methane emissions of 58%.

Permafrost is also the foundation for many forests and other ecosystems in the Arctic and Subarctic environments. The thawing of the permafrost underlying these environments in the creation of thermokarst can substantially alter these environments, and in some cases cause a complete conversion from terrestrial ecosystems to aquatic or wetland systems (Murton 2009; Jorgenson et al. 2001; Osterkamp et al. 2000).

2.2.3. Thermokarst and Remote Sensing

Due to the remoteness of the study areas regarding thermokarst, remote sensing is a valuable tool to help study and understand thermokarst activity. Several studies have been performed using aerial photos and satellite imagery to identify and understand the processes behind thermokarst activity.

Medium resolution data, such as Landsat and Multispectral Scanner (MSS) imagery has been used in several studies involving large study areas. Landsat Thematic Mapper (TM) 5 imagery was utilized to find lake expansion and breaching along the Arctic coast of Alaska. This research created a land and a water mask from a 1985 and a 2005 image and subtracted the two images to find areas where land was accreted and submerged (Mars and Houseknecht 2007). Hinkel et al. (2005) also used Landsat mosaics from the 1970s and 2000 to determine where lakes are disappearing. By

creating polygon shapefiles of the lakes in each of the mosaics and then subtracting the two shapefiles, the researchers were able to determine where lakes disappeared. Smith et al. (2005) also studied lakes in Siberia utilizing MSS imagery from 1973 and Russian RESURS-1 imagery from 1997, finding that 125 lakes vanished.

Finer resolution imagery and photography are also utilized in many studies to identify thermokarst events over smaller areas. Yoshikawa and Hinzman (2003) used 1950 and 1981 aerial photographs and 2000 IKONOS imagery to identify changes in 24 individual ponds near Council, Alaska. Inspection of the images showed that of the 24 ponds, 20 decreased in size between 1950 and 1981 and 22 decreased in area between 1950 and 2000. Declassified CORONA images were used in another study to complete high-resolution mapping of thermokarst activity in Northeastern Siberia (Grosse et al. 2005). This method was able to identify 16 thermokarst depressions and a total of 20,500 water bodies. This study did not try to identify or quantify change; it only examined images from one point in time, so it was only seeking to identify these features on the landscape. Another study by Vallee and Payette (2007) analyzed three lakes in Northern Quebec using 1957 aerial photographs and a map of the mineral palsas, thermokarst ponds, and river shores provided by a total station. The study found an increase in thermokarst pond area of 76 percent. All of these varying results from both fine resolution imagery and medium scale imagery, increases in lake area and

decreases in lake area, demonstrate the variety of manifestations that thermokarst can have on the landscape.

Regardless of the resolution of imagery used, all of the studies regarding thermokarst activity and thermokarst change involved multi-temporal analyses of satellite imagery and aerial photography, as is required to assess any changes on the landscape over time. Automatic change detection techniques, such as post-classification change detection and image algebra, are useful for assessing and monitoring changes over large areas (Kaab 2008).

Even though remote sensing is helpful in locating, quantifying, and assessing thermokarst change on the landscape, it is not without its difficulties. Firstly, thermokarst manifests in a variety of different ways, with different time scales and sizes, potentially requiring images of different spatial resolutions. Thermokarst activity may also be difficult to detect, because it has a variety of spectral characteristics (Jorgenson et al. 2008). For example, it may have a spectral signature similar to that of barren land or it could manifest as an increase or decrease in a lake's area. These difficulties in thermokarst remote sensing are in addition to the general difficulties experienced in Arctic remote sensing.

2.3. Remote Sensing in the Arctic

Due to its extreme location and difficult accessibility, the Arctic is a difficult area to research. Remote sensing is a valuable tool to Arctic researchers, allowing them to obtain important information and trends without having to be present; however, remote sensing in the Arctic is not without its challenges.

2.3.1. Problems and Issues

One major challenge regarding remote sensing in the Arctic is the lack of long term datasets. The largest datasets include the Landsat Multispectral Scanner (MSS), with imagery available from 1972 to 2000, and the Advanced Very High Resolution Radiometer (AVHRR) imagery, with imagery from 1982 until present. However, the characteristics of these sensors are not optimal for research in the Arctic (Stow et al. 2004).

The Arctic poses many physical challenges to obtaining remote sensing imagery. There are issues with a short growing season, cloud cover, solar geometry, and snow and ice cover. The growing season only lasts approximately two to four months, which makes it difficult to acquire adequate imagery for classification and change detection analyses. The short growing season also can be coupled with the persistent cloud cover to increase the difficulty of Arctic remote sensing. Additionally, the Arctic is

characterized by low solar angle, which makes shadows another challenge attributed to Arctic remote sensing. Additionally, ice and snow cover can mask certain spectral signatures of importance, such as vegetation, to researchers in this environment (Stow et al., 2004).

2.3.2. Land Use/Land Cover Changes

Many attempts have been made to classify the land cover of the Arctic landscape, using a plethora of different remote sensing techniques. Balser and Walker (2003) created a vegetation map using Landsat MSS images from 1976 to 1982, supplemented by aerial photography and low-level helicopter flights. The vegetation classification scheme was derived by the researchers. In a case study by Tweedie and Noyle (Stow et al. 2004), IKONOS images were used to ascertain land cover change. Using a supervised classification with seven major and fifteen minor classes, Barrow, Alaska, was classified. Another case study by Verbyla et al. (in Stow et al. 2004) utilized Landsat Thematic Mapper (TM) imagery to detect land cover changes, such as increased shrub cover. Post-classification change detection was performed on unsupervised classifications of two images; however, the classification scheme used was not enumerated. All of these case studies show the need for a more uniform land cover classification scheme for the Arctic, for each study used a different classification scheme. The lack of a uniform scheme is impeding progress working towards

understanding changes throughout the Arctic. Walker et al. (2002; p 4551) indicate the need for a global land cover map of the Arctic for ". . . global-change and conservation studies, land-use planning, large-scale resource development, and education." Walker et al. (2002) present the six-subzone Circumpolar Arctic Vegetation Map (CAVM) created from AVHRR imagery in an attempt provide a more universally accepted classification scheme for the arctic.

Despite these issues with land cover classification in the Arctic, vegetation trends have still been noted by many researchers. Racine et al.'s case study (in Stow et al. 2004) utilized repeat photography to document differences in vegetation on Alaska's North Slope. This study found that over half of the 236 photographs showed an increase in shrub cover. Chapin et al. (2005) also found a 1.2% per decade increase in shrub cover on the North Slope of Alaska since 1950. Ahou and Myeni (in Stow et al. 2004) also found an increase in photosynthetic activity over the past 18 years by using NDVI data. Jia et al. (2003) also indicated a general trend of increasing NDVI on the North Slope of Alaska.

2.4. Image Processing Programming and Feature Extraction

Image processing programming and feature extraction are often discussed together, for many researchers would like to automatically or semi-automatically

extract features. In order to do this, a program or algorithm must be used that distinguishes that particular feature from the other features present on the image.

2.4.1 Image Processing Programming

Programming image processing algorithms have been completed in a variety of programming languages, such as FORTRAN, C, C++, and Visual Basic. Researchers have created programming languages that make programming easier to understand and create algorithms. One such instance is the visual programming language VIVA for image processing (Tanimoto 1990). Though this programming language is easy to understand and learn, it is not compatible with such software as ERDAS and ArcGIS, limiting its application to spatial phenomena. Both ERDAS and ArcGIS have programming capabilities imbedded. Using the ERDAS Developer's toolkit, programmers can customize and adapt existing algorithms to solve individual problems using the C++ programming language. Though ArcGIS's image processing capabilities are limited, image processing programming is still possible using the Visual Basic programming language.

2.4.2 Feature Extraction

Automatic detection of features on satellite imagery has been a topic of research for many years and has yielded several different potential methods for extracting different entities. Extracting features is typically based on the similarity and differences between adjacent pixel values. Methods of feature extraction include:

1. Thresholding, where a certain value is used as a threshold to separate the feature from the background;
2. Polygonal extraction, where texture (coarseness, contrast, roughness, etc.) are used to extract the features; and
3. Edge detection, where sharp changes in pixel values are detected to determine the edges of a linear feature or the edge of a feature (Armenakis and Savopol n.d.)

There are many examples of feature extraction in urban applications, such as the extraction of roads and buildings. Environmental applications of automatic extraction are not as plentiful. For automatic extraction of craters from panchromatic images of various planets, Urbach and Stepinski (2009) used several filters to remove unnecessary data from the images, which were followed by a supervised classification. This, however, is only semi-automatic extraction, since user selection of the training sites is required for the supervised classification, and this process also requires a considerable

amount of time. In order to extract individual trees from high resolution satellite images, Wolf & Heipke (2007) utilized geometry properties as well as radiometric properties (Normalized Difference Vegetation Index) to extract the trees; however, this required three steps and a digital elevation model (DEM) in addition to imagery.

2.5. Summary

Though various studies have been completed documenting Arctic climate changes, thermokarst activity, and feature extraction, no studies have examined automatically extracting thermokarst activity. This is likely due to the difficulty of identifying thermokarst solely from satellite imagery, for it manifests in a variety of ways on the landscape. Despite this difficulty, the increasing incidence of thermokarst and its role in Arctic and global climate change cannot be disputed, and its rapid identification is necessary to further understand the phenomenon (Murton 2009; Osterkamp 2005; Jorgenson et al. 2001; Osterkamp et al. 2000; Romanovsky et al. n.d.).

CHAPTER III

METHODS

Remote sensing is a valuable asset in assessing changes in the Arctic. Many locations in the Arctic are difficult to access, and remote sensing allows researchers to view the landscape without having to be present. Also, it allows researchers to be able to see Arctic environments at a scale that makes it easier to locate and assess changes on the landscape. This chapter details the previous methods utilized by other researchers and the methods utilized in this research.

3.1. Previous Change Detection Methods and Application Development

There are many different types of change detection techniques that researchers use to determine changes between two or more images taken at different times. Each method has their advantages and disadvantages. Such change detection techniques include write function memory insertion, multi-data composite image, image algebra (i.e. band differencing), post-classification comparison, binary mask applied to date 2, ancillary data source used as date one, and many others. One of the most commonly used techniques for change detection is the post-classification comparison, for it

provides quantitative “from-to” information. Though the “from-to” information provided by this technique is one of its advantages, there are disadvantages. The post-classification comparison technique requires the classification of both the before and after image, which means the change detection is only as accurate as the respective classifications. Also, it requires two separate classifications, which can be time consuming to create (Jensen 2005).

Automation of the change detection process and automatic detection of features on satellite imagery has been a topic of research for many years and has yielded several different potential methods for extracting different entities. For automatic extraction of craters from panchromatic images of various planets, Urbach and Stepinski (2009) used several filters to remove unnecessary data from the images, which were followed by a supervised classification. This however, is only semi-automatic extraction, since user selection of the training sites is required for the supervised classification, and this process also requires a considerable amount of time. In order to extract individual trees from high resolution satellite images, Wolf & Heipke (2007) utilized geometry properties as well as radiometric properties (Normalized Difference Vegetation Index) to extract the trees; however, this required three steps and a digital elevation model (DEM) in addition to imagery. This research hopes to require only satellite imagery (to increase usability and potential users) and fewer processing steps (to increase efficiency).

3.2. Data Sources

For this research, several types of imagery were used for four watersheds (Campsite Lake, NE-14, I-Minus, and 120) with known thermokarst activity in the Upper Kuparuk River Region (Figure 3.1). These images were used to extract spectral information about thermokarst and water features that were used in extracting and identifying potential areas of thermokarst activity. Fine (sub-meter to 20-meter) and medium (20 to 100-meter) resolution imagery were utilized. The imagery included a 1978 False Color Infrared (CIR) Aerial Photographs, a 2005 Satellite Pour l'Observation de la Terre (SPOT) image, and 2001, 2002, and 2006 Histogram Equalized Landsat TM images.

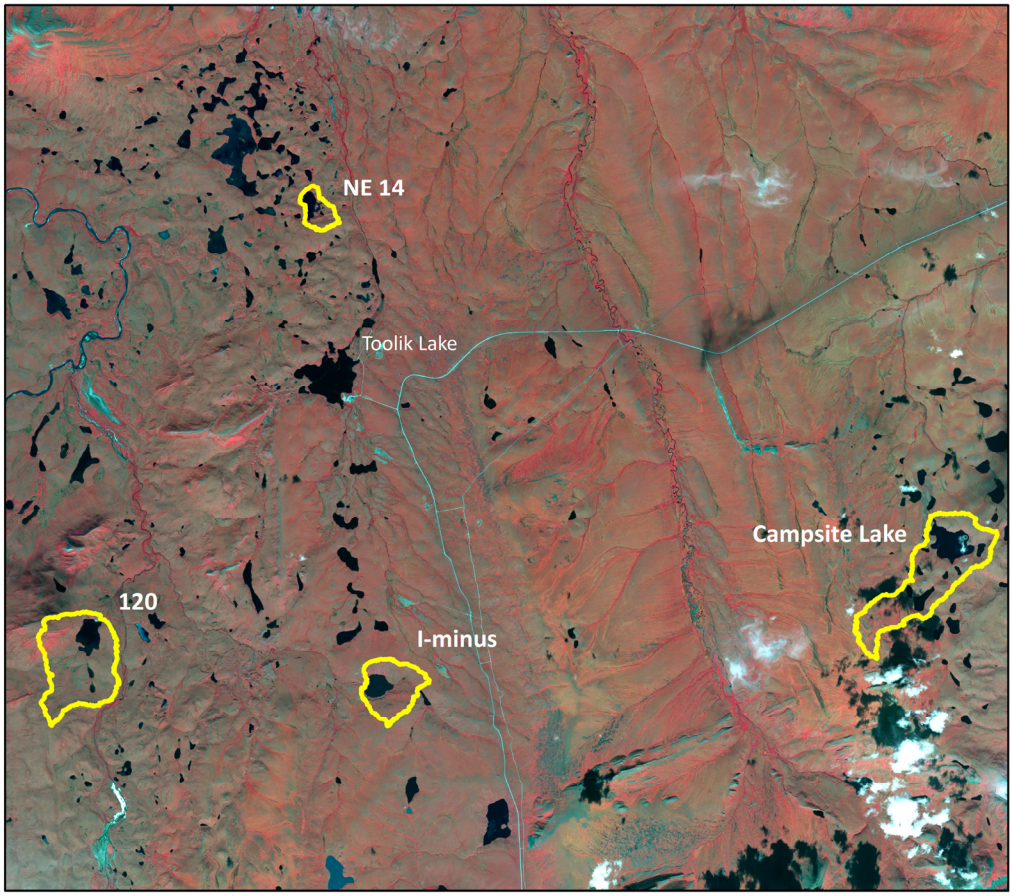

Figure 3.1. Watersheds of Interest.

The various Landsat TM images were acquired from United States Geological Survey (USGS) Earth Resource Observation and Science (EROS) located in Sioux Falls, South Dakota. The Landsat images have spatial resolutions of 30 meters, with a temporal repeat cycle of 16 days. The Landsat images have seven spectral bands. Each band on the Landsat Thematic Mapper (TM) sensor corresponds to certain portion of the electromagnetic (EM) spectrum. Only three bands were of particular interest in this research: bands four, three, and two. These were the bands of interest, because they

correspond to the three bands available in the other images utilized by this research. Band four corresponds to the near-infrared portion of the EM spectrum, with wavelengths ranging from 0.76 to 0.90 micrometers (μm). Band three corresponds to the red band, with wavelengths ranging from 0.63 and 0.69 μm. Finally, band two corresponds to the green portion of the EM spectrum, with wavelengths ranging from 0.52 to 0.60 μm (USGS 2010). The CIR aerial photographs were acquired on August 26, 1978, and have a spatial resolution of 2 meters. The CIR aerials contain three bands: near-infrared, red, and green. The 2005 SPOT image, acquired in July 2005, from the SPOT Corporation, has a spatial resolution of 5 meters (after merging a 10-meter multispectral image with a 2.5-meter panchromatic image), consisting of similar spectral bands as the CIR aerials, with near-infrared, red, and green bands.

3.3. Preprocessing of Imagery

The application developed in this research sought to automatically detect thermokarst, but certain preprocessing of the imagery was required for an accurate assessment of the imagery. For example, all of the imagery utilized by the program required the same projection. If the images were not in the same projection, they needed to be rectified, so that the places on the images correspond correctly with respect to each other (Jensen 2005). One must also be aware that if the images are not correctly rectified, the change detection may show extraneous changes (Figure 3.2).

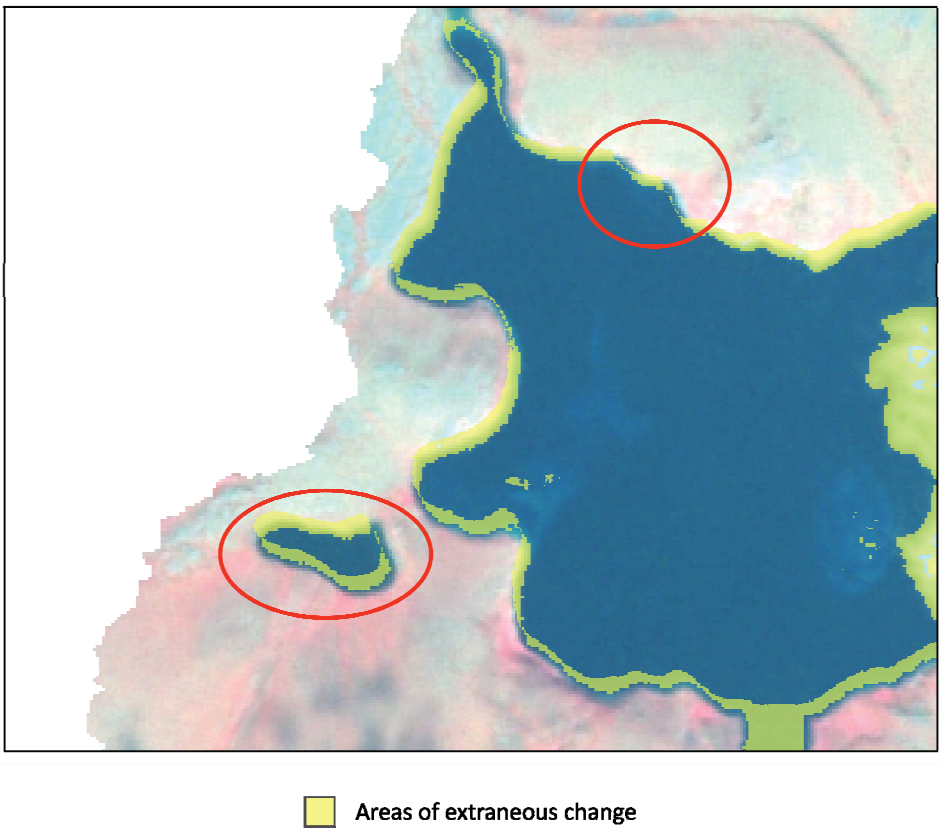

Figure 3.2. CIR-SPOT Change detection for Campsite Lake, showing extraneous changes due to the CIR not being correctly rectified. The red circles show where it is particularly evident.

Additionally, the images were subset to the same geographic areas of interest (AOI). If the images did not have the same AOI, the output would not provide a correct examination of the area in the images. As such the information provided by such a change detection may not be sufficiently accurate (Figure 3.3).

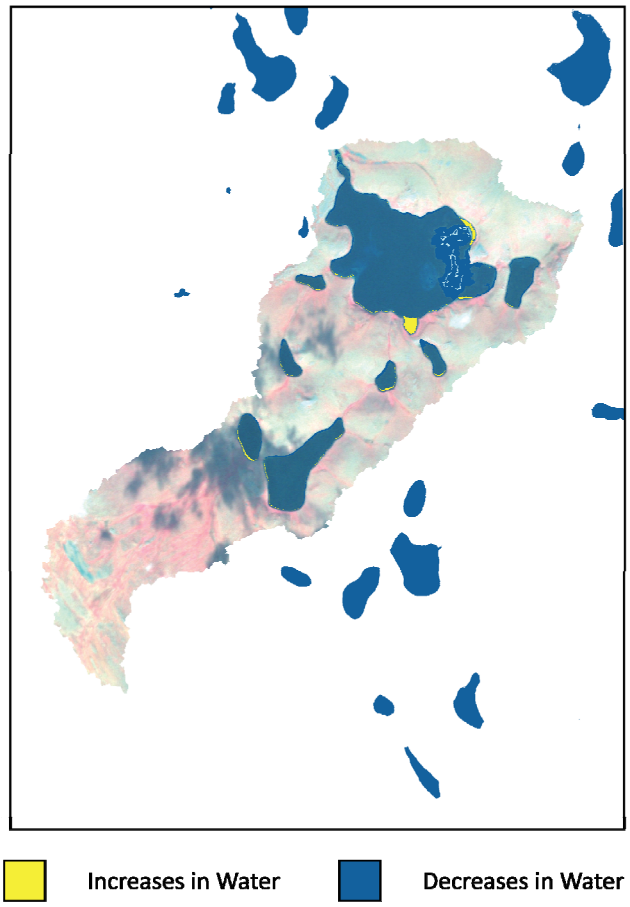

Figure 3.3. Extraneous decreases in water present in a CIR-SPOT change detection of Campsite Lake watershed due to incorrect subset to AOI.

Finally, as a prerequisite for any change detection analysis, the imagery should have the same spatial resolution. In cases where the images are the same spatial resolution, such as if one was assessing a SPOT image to a SPOT image of another year with the same 5-meter X 5-meter spatial resolution, the images do not require resampling. If the two images have differing spatial resolutions, as is the case if one were assessing one SPOT image (5 X 5 m) and one Landsat image (30 X 30 m), the images need to be resampled to a predetermined representative minimum mapping

unit. In this case, the Landsat image may be resampled to the 5 X 5-meter resolution; however, it must be kept in mind that the Landsat data was acquired at a 30 X 30-meter resolution and cannot be expected to be accurate to a 5 X 5-meter resolution (Jensen 2005).

3.4. Methods Utilized in this Research

3.4.1. Spectral Signature Analysis

The spectral signature of a feature, also called its "spectral profile," is the brightness value (BV) for a given pixel (feature) using all of the bands present in the image. The spectral signatures can also be utilized to differentiate features from one another (Jensen 2005). It was important to differentiate between the different features, especially since many features have similar spectral signatures. Since thermokarst can manifest as both water and a barren-like signature, it was important to locate thermokarst both spectrally, as well as spatially. Since various images from different sensors were utilized by this research, as well as other researchers interested in thermokarst activity, it was also important to recognize the spectral differences present in imagery obtained from different sensors. As such, each sensor, Landsat, CIR aerial photographs, and SPOT was evaluated for these spectral differences.

Zonal statistics were used to ascertain the spectral information from each of the images. Zonal statistics require a region, where the output creates information based on the target pixels within said given region (DeMers 2002). Zonal minimum, maximum, and range of each band of each image were the statistics of interest in this research. The zonal minimum examines the zone and returns the lowest brightness value in that zone. The zonal maximum does the same, except providing the highest brightness value in that zone. The zonal range supplies the difference between the highest and lowest brightness values within the zone. The zones to determine these statistical values were based shapefiles of areas of interest (areas of known thermokarst activity and water on the various images) (Figure 3.4). The determined zonal minimums and maximums were then applied as criteria for selecting pixels within those ranges in the entire image. If the range of values was too large, thus selecting areas that were not thermokarst or water, the ranges were refined by analyzing the brightness values of single pixels of known thermokarst activity for the spectral signature of those particular pixels to reduce the amount of extraneous pixels extracted (Figure 3.5).

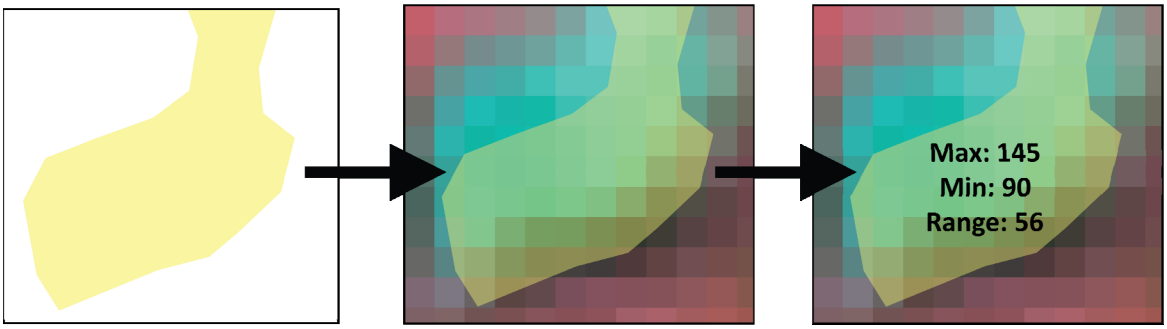

Figure 3.4. Image zonal statistics from shapefiles of areas of interest.

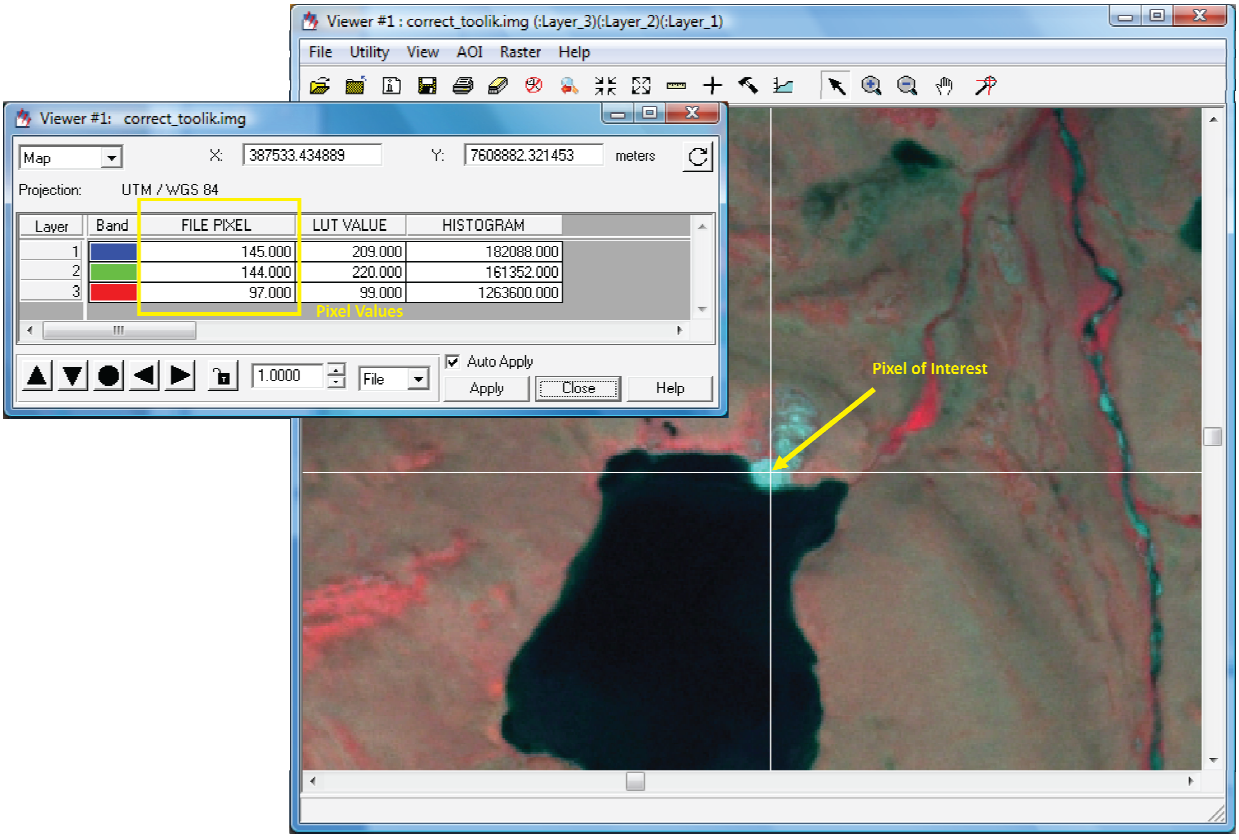

Figure 3.5. Refining the zonal statistic ranges by examining individual excluded pixels for pixel values.

SPOT Image

The spectral ranges for both thermokarst and water were able to be detected from the SPOT images. The spectral range for thermokarst in the near-infrared band was from 90 to 145. The brightness values in the red band were from 115 to 150, and the green band brightness values ranged from 50 to 110. For the water class, the brightness values for the near-infrared band ranged from 57 to 83. The red band brightness values ranged from 36 to 70, and the brightness values in the green band ranged from 10 to 24 (Table 3. 1).

Class	Near-Infrared	Red	Green
Thermokarst	90-145	115-150	50-110
Water	24-30	21-30	17-25

Table 3.1. Range of brightness values for the SPOT image.

Landsat Images

The spectral ranges for the Landsat images were also able to be extracted for both thermokarst and water. Three different histogram equalized Landsat TM (2001, 2002, and 2006) images were used for the extraction of the spectral ranges to ensure that the ranges for the Landsat imagery were not "year-dependent." For the Landsat thermokarst class, the range of brightness values for the near infrared band was from 129 to 194. The red band had brightness values for the thermokarst class ranging from 202 to 234, and the green band had brightness values ranging from 195 to 231. For the

Landsat water class, the brightness values for the near infrared class were from 99 to 128. The red band had brightness values for the water class ranging from 99 to 126, and the green band had brightness values ranging from 99 to 128 (Table 3.2).

Class	Near-Infrared	Red	Green
Thermokarst	129-194	202-234	195-231
Water	99-128	99-126	99-128

Table 3.2. Range of brightness values for the Landsat classes.

CIR Aerial Photographs

Unlike the SPOT and Landsat images, both thermokarst and water class spectral ranges were not able to be extracted from the CIR aerial photographs. For the CIR aerial photograph water class, the range of brightness values for the near infrared band was from 9 to 45. The red band had brightness values for the water class ranging from 0 to 74, and the green band had brightness values ranging from 10 to 24.

The spectral ranges for the thermokarst class were not able to be determined for the CIR aerial photographs. Firstly, there were very few areas in the 1978 photographs that would be considered the barren-like manifestation of thermokarst activity. Of the four watersheds of interest in this study, only the I-minus watershed exhibited this manifestation. The lack of this manifestation made it difficult to accurately portray the ranges on this particular form of imagery. Additionally, the spectral ranges determined from this area also presented challenges. The range of brightness values for near-

infrared for thermokarst in the CIR aerial photographs was from 209 to 253. The red band brightness values ranged from 123 to 223, and the green band brightness values ranged from 111 to 216. When these spectral ranges from the I-minus watershed are applied to that and other CIR aerial photos, many other areas are extracted that are not thermokarst (Figure 3.6). This could be very problematic when looking at two images to determine landscape changes. The analyst might think that there are thermokarst activity and thermokarst changes, when there was not any thermokarst activity at all. For this reason, the thermokarst class was eliminated from the CIR aerial photograph model and only water and other land were considered.

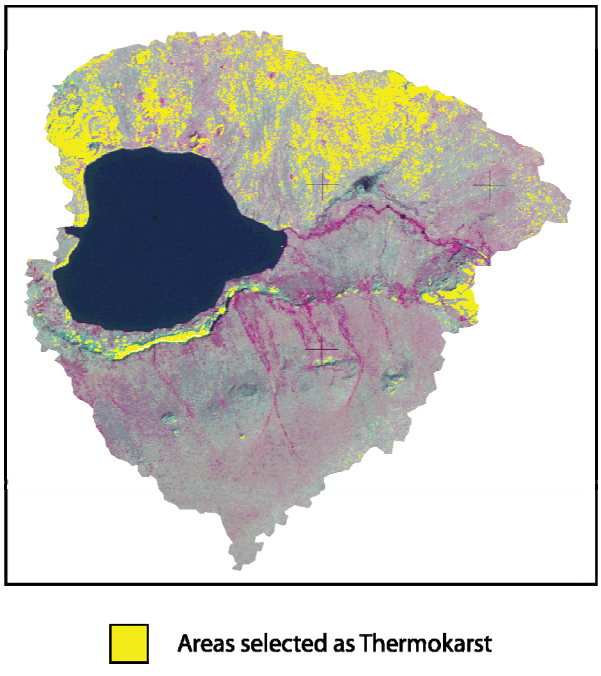

Figure 3.6. Areas in CIR aerial photograph extracted as thermokarst activity.

Challenges With All Images

In all of the images, the thermokarst class consisted of barren-like spectral ranges, and these ranges were similar to many other classes in the Arctic. For example, roads and other infrastructure are features that have a spectral signature within the spectral ranges determined for the thermokarst class (Figure 3.7). This may cause confusion as to what is actually "thermokarst" and what is "infrastructure" if the user's study area is an urban setting. Additionally, mountains and other barren areas are often confused for the thermokarst class.

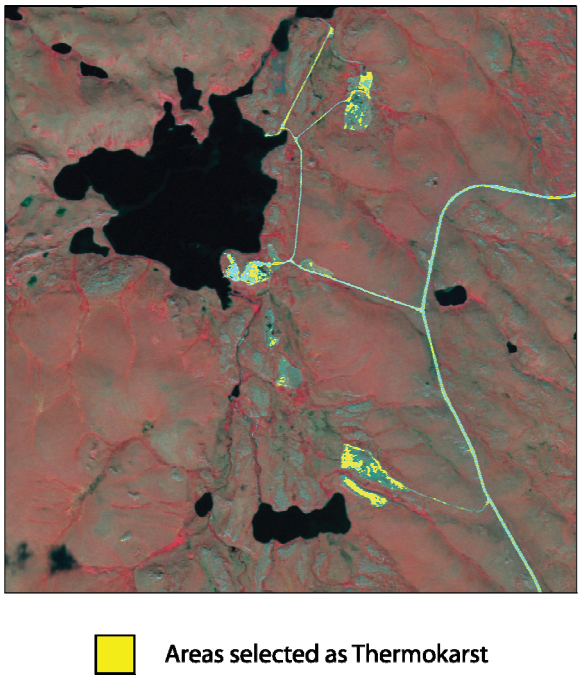

Figure 3.7. Infrastructure being selected as thermokarst activity in the SPOT image.

While water is by far much easier to spectrally differentiate than thermokarst activity, it, too, has its challenges. Water has spectral similarities to shadows. If one of the images utilized in the model has shadows present, then they may be classified similar to water. This is especially true for the Landsat imagery (Figure 3.8). This, like the problems with extracting thermokarst, would produce problems with the change detection and extraneous changes.

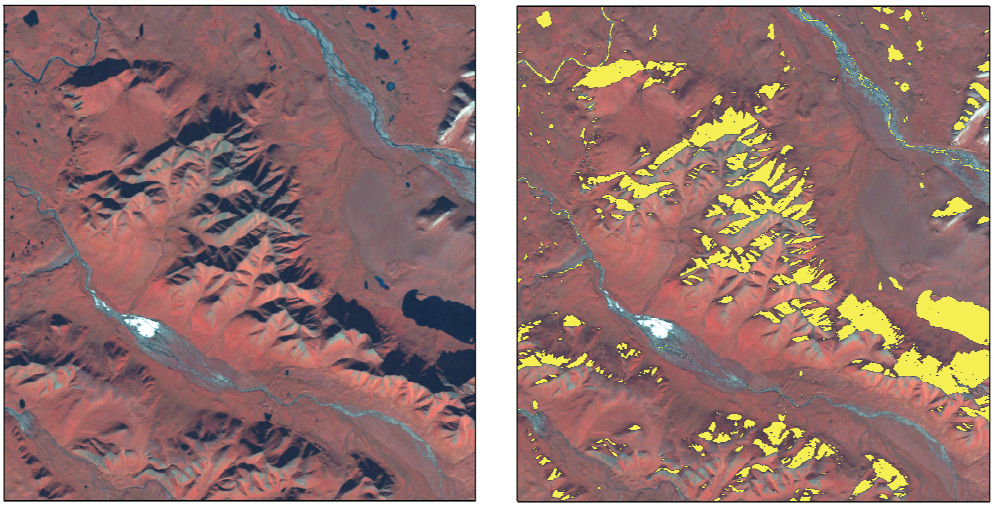

Figure 3.8. Shadows being extracted as water in the 2006 Landsat Image.

3.4.2. Classification

This research utilized a classification process that was similar to supervised classification, which typically requires the utilization of training sites as a means of classifying an image (Jensen 2005). The spectral information for the assorted sites was

applied to the images in a pixel-by-pixel classification to extract the classes of interest. The specific classes of interest were Thermokarst, Water, and Other. The "Other" category encompassed all other features, such as vegetation, that are not within the spectral ranges for the two particular classes of interest. These were the only categories utilized by this research, but they are the only categories of interest in locating areas of thermokarst activity. This research was not interested in locating increases or decreases in Arctic vegetation, such as shrubbery or moist acidic tussock tundra, only in locating areas of thermokarst activity. From the spectral ranges determined by the spectral analysis of each image, the pixels contained in each of these three classes were assigned a numerical value. Water was given the numerical value of one; thermokarst was given the numerical value of three, and the other class was given the numerical value of six (Figure 3.9).

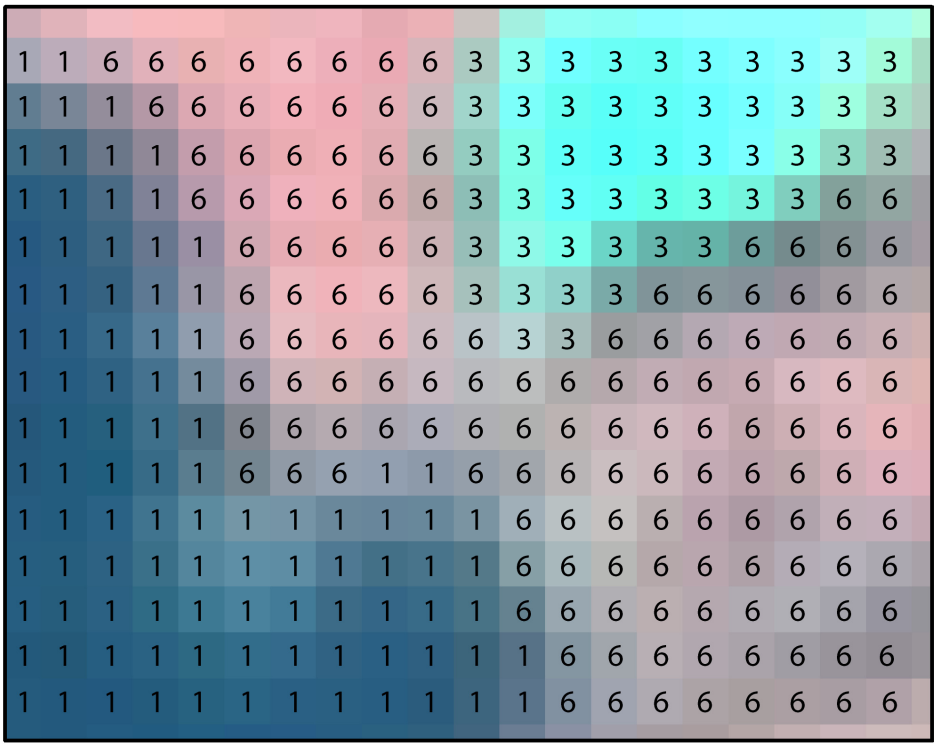

Figure 3.9. Assigning numerical values to spectral ranges.

3.4.3. Change Detection

This research utilized a change detection method that was similar to post-classification comparison in that it required classifications of two images and compared the classifications. The numerical classification of an after image was subtracted from the classification of a before image to provide information assessing if and how the area changed (Figure 3.10). The resulting numerical values detailed if an area changed from land to water or if no change occurred at all (Table 3.3).

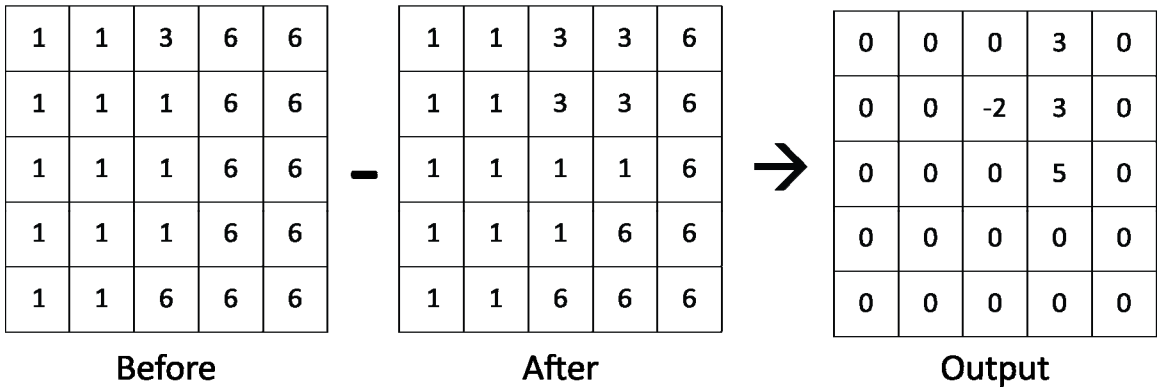

Figure 3.10. Example of numeric image subtraction.

Before Image Value	After Image Value	Yields	Indicates
Water = 1	3	-2	Thermokarst where there was water previously.
1	1	0	No change.
1	6	-5	Decrease in amount of water.
Thermokarst = 3	1	2	Water where there was thermokarst previously.
3	3	0	No change.
3	6	-3	Another land use where there was thermokarst previously.
Other = 6	1	5	Increase in amount of water.
6	3	3	Potential thermokarst where there was not previously thermokarst.
6	6	0	No Change.

Table 3.3. Meanings of numerical values of the change detection.

3.5. ERDAS Developer's Toolkit

The ERDAS Developer's Toolkit uses the C or C++ programming language and includes application programming interfaces (APIs) to be modified for the user's specific needs (Leica Geosystems Geospatial Imaging 2008). The toolkit allows for both customization and extending. Customization in IMAGINE includes editing the preferences and the existing EMLs. However, when editing the EMLs the commands cannot be changed. Extending in IMAGINE includes editing existing scripts, creating new Spatial Modeling Language scripts, or creating an entirely new application. This research will focus on extending use of IMAGINE, including creating new EMLs and SMLs (ERDAS Online Help).

3.5.1. Spatial Modeling Language (SML)

IMAGINE's Model Maker allows the user to create a model that is not offered by the default software or modify an existing model. Functions and criteria can be created or edited using mathematical expressions. Of particular interest was the ability to create a model specifying spectral criteria for each sensor using cell values (Figure 3.11). Using algebraic equations to specify the criteria for each band and each class, the model can select and identify pixels within those ranges and give all other pixels another value. Once the model is refined, a script was generated that was then used in an existing EML.

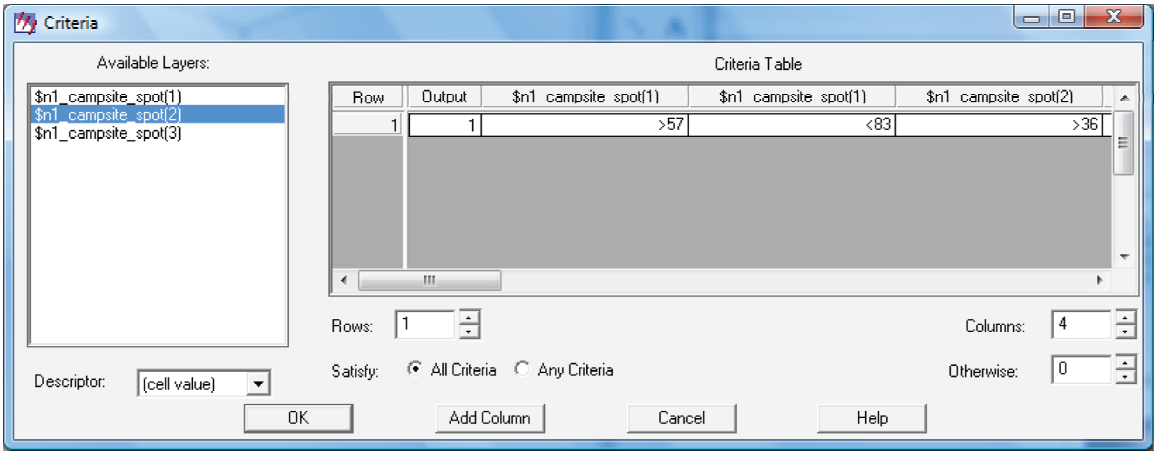

Figure 3.11. Dialog allowing the declaration of one or more criteria to classify imagery.

SPOT Images

The SPOT model created has three components: an input image (SPOT Image), the criteria, and an output image (Figure 3.12). If a pixel in band 1 had a brightness value of greater than 57 and less than 83, and in band two of greater than 36 and less than 66, and in band three of greater than 17 and less than 24, then those pixels were assigned a value of 1 for water. If a pixel in band 1 had a brightness value of greater than 90 and less than 145, and in band two of greater than 115 and less than 150, and in band three of greater than 50 and less than 100, then those pixels were assigned a value of 3 for thermokarst. Otherwise, the pixels were assigned a value of 6. The output was an unsigned 8-bit thematic raster image.

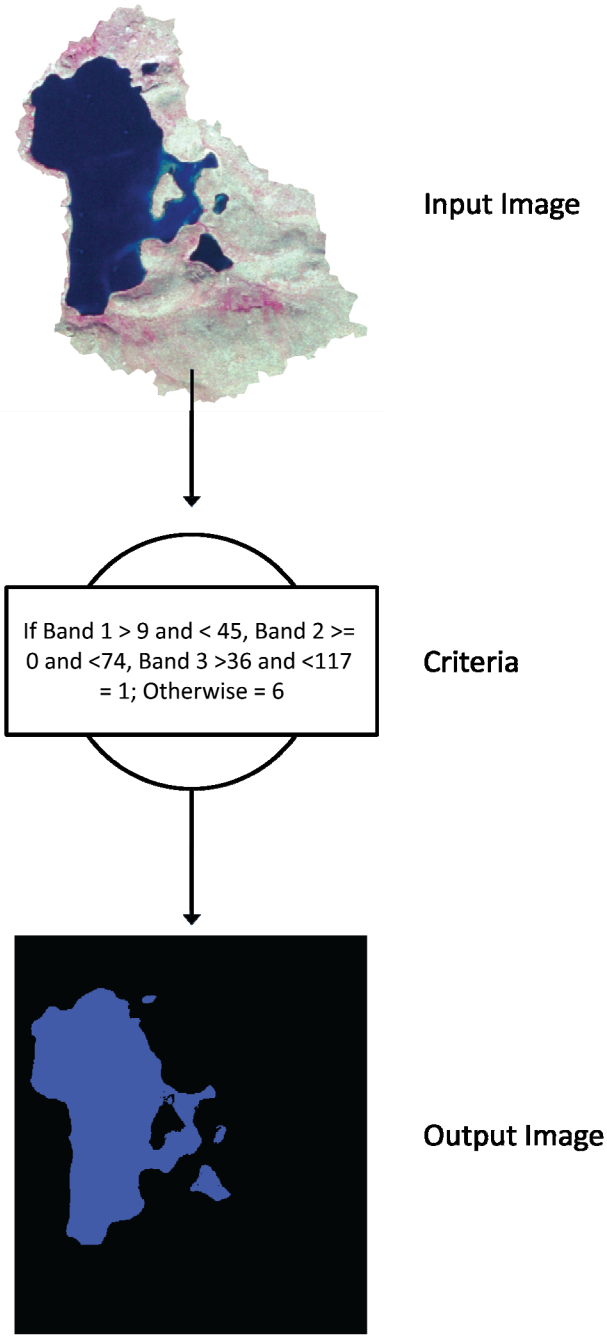

Figure 3.12. Model components for the SML classification for extracting water.

Landsat Images

The Landsat image model also contained the three components of the other two models. The input for this model was a Landsat image. Like the SPOT imagery, the Landsat model had criteria for both water and thermokarst. If a pixel in band 4 had a brightness value of greater than 129 and less then 194, and in band 3 of greater than 202 and less than 234, and in band 2 of greater than 195 and less than 231, then the pixel was assigned a value of 1 for water. If a pixel in band 4 had a brightness value of greater than 99 and less than 128, and in band 3 of greater than 99 and less than 126, and in band 2 of greater than 99 and less than 128, then the pixel was assigned a value of 3 for thermokarst. If the pixel was not met by any of these criteria, it was assigned a value of 6. Like the other models, the output of this model was an unsigned 8-bit thematic raster image.

CIR Aerial Photographs

The difficulty in determining the spectral ranges for the barren-like manifestation of thermokarst from the CIR aerial photographs prevented the use of such a range in the CIR Aerial Photographs classification model. As such, only water was utilized in the model for the classification of these images. Despite not having the thermokarst class, the model still runs. Instead of having three numerical classes,

however, it only has two: one and six. The only criteria necessary were the three bands for water. If a pixel in band one had a brightness value of greater than 9 and less than 45, and in band two of greater than 6 and less than 74, and in band three of greater than 36 and less than 117, than those pixels were assigned a value of 1. Otherwise, the pixels were assigned a value of 6. The output was an unsigned 8-bit thematic raster image, with a name of the user's choice.

Change Detection Subtraction

Once the models for the individual types of imagery were created, they can be put together and rearranged to form the change detection model. There were only two additional components to the change detection model from the imagery classification models. These components were a new function and a new output (Figure 3.13). The classification models were put into a before and after category. The outputs of the classification models were converted into temporary integer raster images, which only temporarily stored the classifications until the model was completed. In the new function, the after image classification was subtracted from the before image classification. The output must be a signed raster image, because to understand the subtraction, negative values must be represented in the output. For the change detection models in this research, signed 8-bit continuous raster outputs were used.

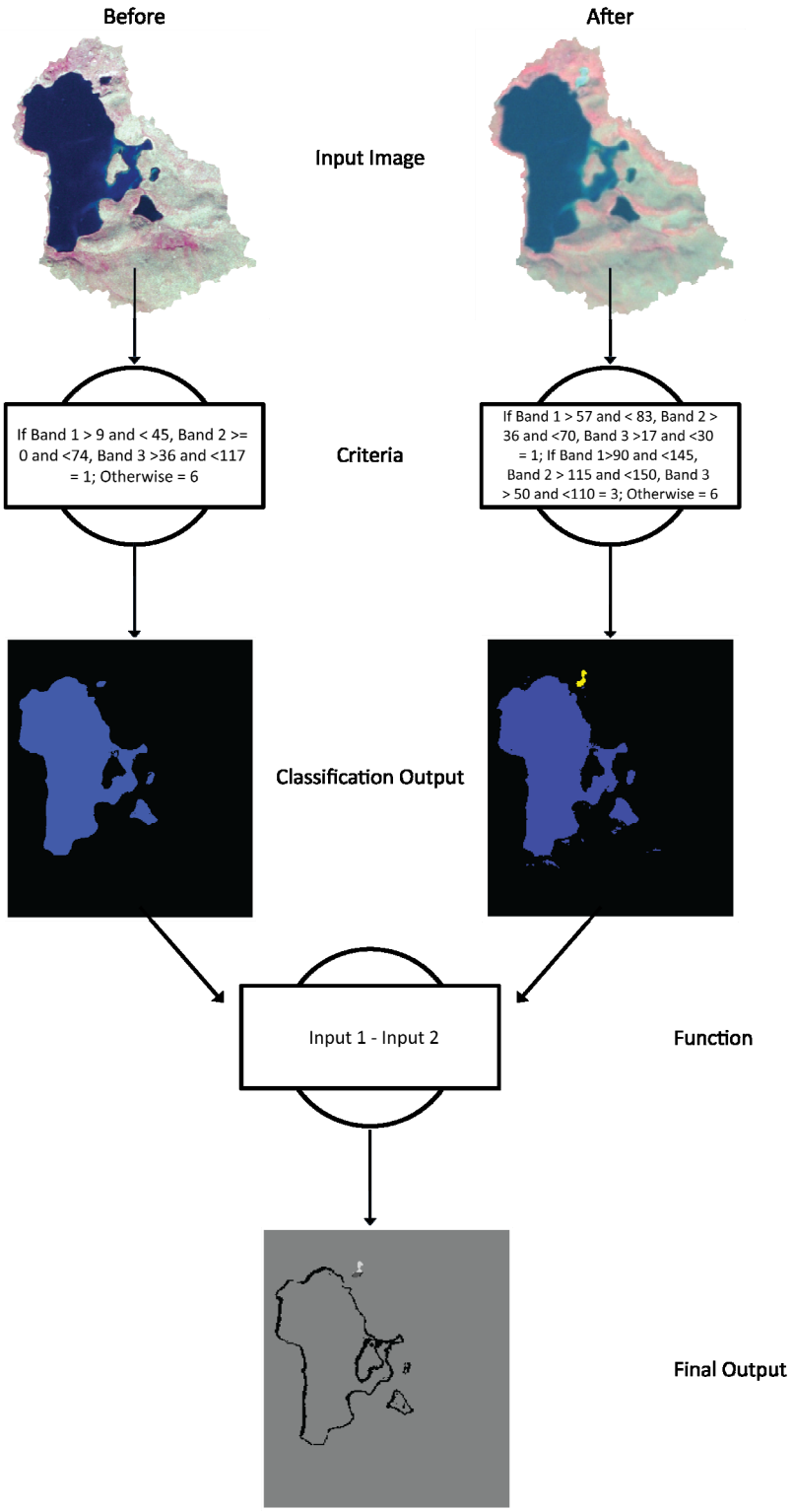

Figure 3.13. Example of an SML model for the subtraction change detection performed.

3.5.2. ERDAS Macro Language (EML)

EML was used for creating the Graphical User Interfaces (GUIs) for IMAGINE, and it served as both a scripting language and a user interface language. This means that with EML the user can define the actions to be taken as well as interact with the interface. To create the GUI using EML, one must create a code detailing how the GUI should look, how big it should be, what elements should be contained in it, and the spacing of the elements (Figure 3.14). Example elements include buttons, checkboxes, file names, groups, lines, popup lists, radio buttons, and countless others. ERDAS recommends using Open Office Draw to layout the GUI before creating the code for the EML. This not only allows for the organization of all the elements, but it also allows for the obtainment of size and location values that are required for the geometry declaration in the EML code. The geometry measurements are in pixel; however, since there is no pixel option in Open Office Draw, “points” are used. Once the code is compiled, it creates the GUI described (ERDAS 2009).

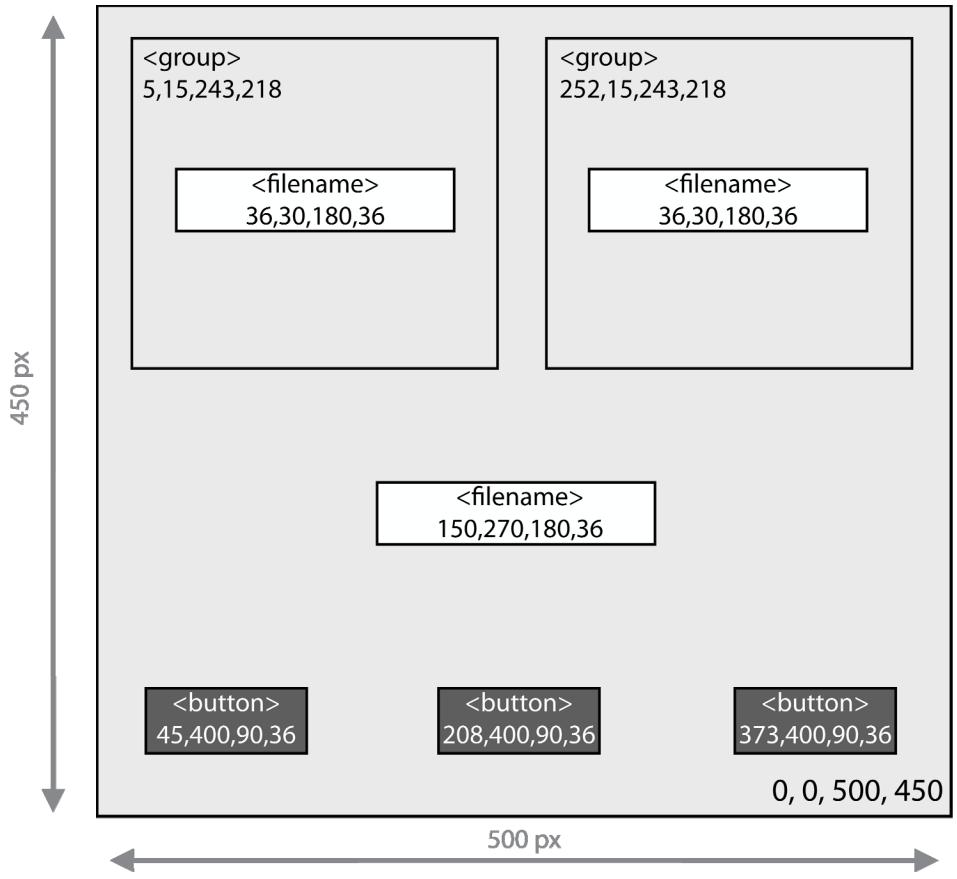

Figure 3.14. Example GUI schematic drawing used to create a GUI code in EML.

There were several elements to the GUI that needed to be included in the code. These elements included the frame, two groups, three filenames, two popuplists, and three buttons. The frame of the program is the rectangular component that contains all of the other GUI frameparts. A group is a framepart that separates its contents from the rest of the frame. Popuplists are lists that when the arrow is clicked, reveals the contents of the list and are able to selected. Filenames are where files can be loaded or created by the program. Finally, buttons are what activate certain processes, such as

unloading the frame (closing) or initiating models (Leica Geosystems Geospatial Imaging 2008). The two groups contained one filename and one popuplist a piece. One group was for "before" images and one group was for "after" images. The popuplists were for the sensor names: CIR, SPOT, and Landsat. The final filename was for the output of the change detection. The three buttons included an "Ok" button, a "View" button, and a "Cancel" button (Figure 3.15). The "Ok" button was disabled upon the start up of the program until all of the filenames have been entered. Once the "Ok" button is enabled and selected, it runs a model based on the user inputs. If the user selected that they have entered two Landsat images into the popuplists, then the model for a Landsat-Landsat change detection runs. If the user enters a combination of sensors that the program does not recognize, the frame closes. The "View" button opens Erdas's Model Maker and allows the user to see an example of one of the models that are run. Finally, the "Cancel" button unloads the frame. The final output should be loaded into a viewer as a pseudo color image, so that different colors are assigned by the user to the different values of the subtraction. It can be loaded as another file type; however, the other file types do not allow the user to change the colors of the "from-to" classes. The appearance of the GUI is shown in Figure 3.15. To see the full code, see Appendix A. Additionally, a button was created and coded onto the main toolbar of ERDAS to activate the GUI for this program. The button to call the program is displayed in Figure 3.16.

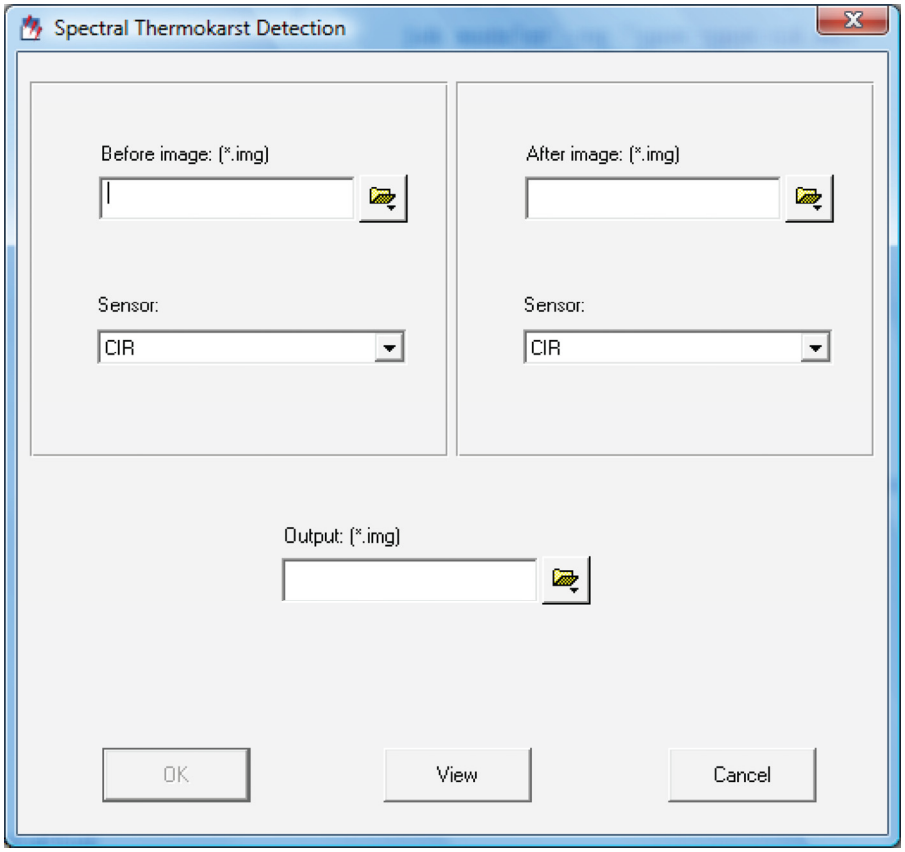

Figure 3.15. GUI as displayed in ERDAS IMAGINE.

Figure 3.16. Button used to activate program.

3.6. Program Testing

Three watersheds with known thermokarst activity and three watersheds without known thermokarst activity were chosen to test the model. The watersheds tested for known thermokarst activity were Campsite Lake watershed, Lake 120 watershed, and NE14 watershed. The three watersheds without thermokarst activity were Lake 100 watershed, Island Lake watershed, and NE8 watershed. Lake 100 was chosen because it does not have any barren areas, just the lake and other vegetation. Island Lake watershed was chosen because they have features that have a "barren-like" spectral signature. For example, Island Lake watershed includes part of the Dalton Highway, as well as some mountainous areas. For each watershed, four trials were run. The first was a CIR aerial photograph and SPOT image change detection. The second was a SPOT image and Landsat image change detection. The third trial was a CIR aerial photograph and Landsat Image change detection. The final trial involved a Landsat-Landsat change detection.

Since each of the images has a different spatial resolution, the images were resampled to match the lowest spatial resolution. For example, the CIR aerial photographs have a spatial resolution of 2-meter X 2-meter and the SPOT images have a 5-meter X 5-meter resolution. In a CIR-SPOT change detection, the CIR was resampled to match the SPOT's 5-meter X 5-meter resolution. In a change detection that involved

a Landsat image, the other image was resampled to match the 30-meter X 30-meter resolution of the Landsat.

3.7. Summary

Many of the methods utilized in this research are not new, but were applied in a new direction. This research sought to utilize remote sensing imagery to identify thermokarst, in its various forms. This research also sought to decrease the amount of time researchers would need to spend assessing imagery to find potential areas of thermokarst to research. To do this, it sought to automatically classify images of a specific sensor using the spectral properties of the classes of interest using a combination of SML and EML in the IMAGINE software, then perform a subtraction change detection on the before and after thematic classifications to find specific areas of interest.

CHAPTER IV

RESULTS

4.1. Results of Preliminary Testing

To ensure the program's usefulness and accuracy, several test watersheds (Lake 120, Campsite Lake, and NE14) were run to determine if the program accurately identifies areas of thermokarst activity. Additionally, three watersheds (Lake 100, Island Lake, and NE8) without known thermokarst activity were assessed, to determine if any extraneous thermokarst areas are detected with the program.

4.1.1. Areas of Known Thermokarst Activity

120 Watershed

The first trial used the CIR aerial photographs and SPOT image. Visual inspection of the CIR aerial photograph showed no pronounced thermokarst activity in 1978; however, on the 2005 SPOT image, an area of thermokarst developed on the northeast shore of Lake 120. The manifestation of thermokarst in this lake is the barren-like manifestation of thermokarst activity. Additionally, a portion of Lake 120 was also converted to this barren-lake manifestation of thermokarst. As such, the CIR-SPOT

change detection model should show an area of thermokarst where there was no thermokarst prior.

The results of this model indeed showed an area of thermokarst activity in the northeast section of Lake 120 (Figure 4.1). Figure 4.1 also shows that while it did indicate an area of thermokarst where there was some other land class previously, it did not extract the entire area. The results of the CIR-SPOT change detection model also correctly indicated areas that were once water, but are now thermokarst (Figure 4.2). Of the 1.5 hectare (ha) thermokarst event, the model was able to correctly identify 0.54 ha (36%), with no incorrect identifications.

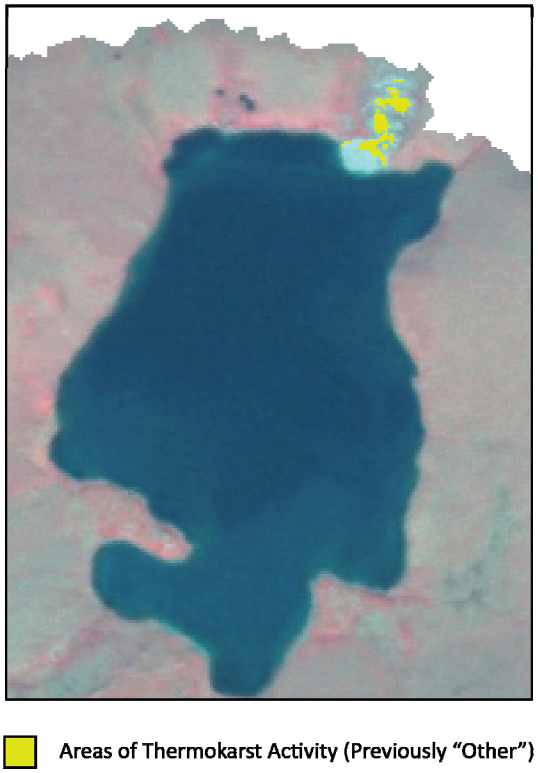

Figure 4.1. 120 Watershed with areas indicated to have thermokarst activity in the SPOT image, but not in the CIR image.

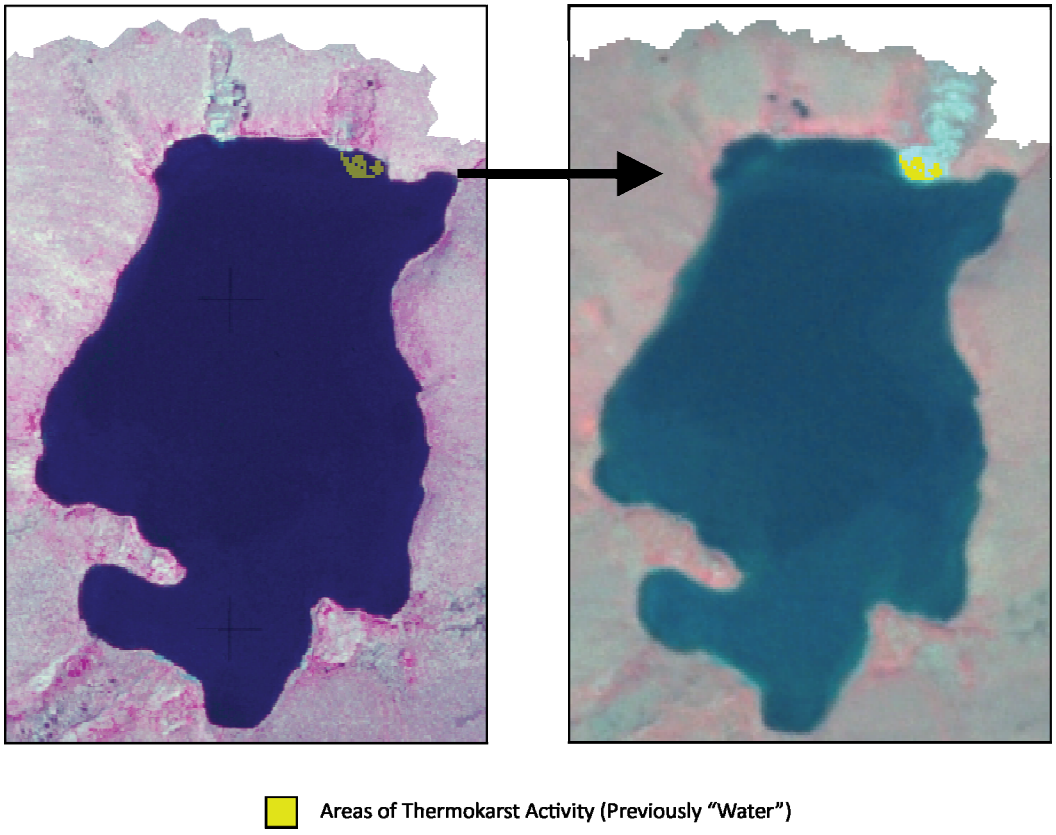

Figure 4.2. CIR (left) and SPOT (right) showing and area of water that was converted to thermokarst and picked up by the program.

One of the problems with this model was that it showed a large decrease in the amount of water (Figure 4.3). Of the 54.4 ha of water in the entire watershed, 4.5 ha was incorrectly shown to be a decrease in water (8.3%). This could be due to several factors or a combination of several factors:

1. Incorrect rectification of images;
2. Scale differences and resampling issues (mixed pixels);

3. Or, those areas of water were not included in the spectral ranges of the model.

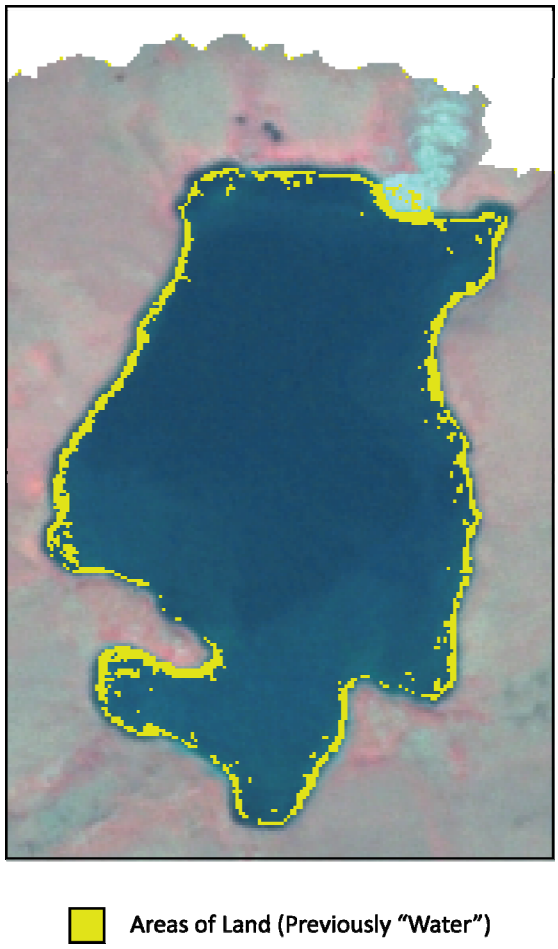

Figure 4.3. Areas indicating an incorrect decrease in the amount of water.

The second trial was the SPOT-Landsat change detection model. Visual inspection of the images utilized shows that both the 2005 SPOT and the 2006 Landsat images show the barren-like thermokarst activity on the northeast section of the lake. Since the model is a change detection; however, the thermokarst area on the 2005 and

2006 images should show up a “no-change” or a few pixels indicating the growth of the thermokarst area. Much like the CIR-Landsat change detection, it was able to detect areas of increased thermokarst activity, but it had problems with the perimeter of the lake (Figure 4.4). Additionally, Figure 4.4 shows (in the red circles) that other landscapes, which are not thermokarst, are being detected as thermokarst activity. Of the 0.99 ha of thermokarst found by this model, 50% (0.49 ha) was not thermokarst. Since the spectral ranges used to identify thermokarst could also identify barren or barren-like features, these extractions could be heath. Heath has a similar spectral signature to that of barren land and thermokarst. Also, of the approximately 54 ha of water present in this watershed, 10.4 ha was incorrectly identified as an increase in water levels (19.3%).

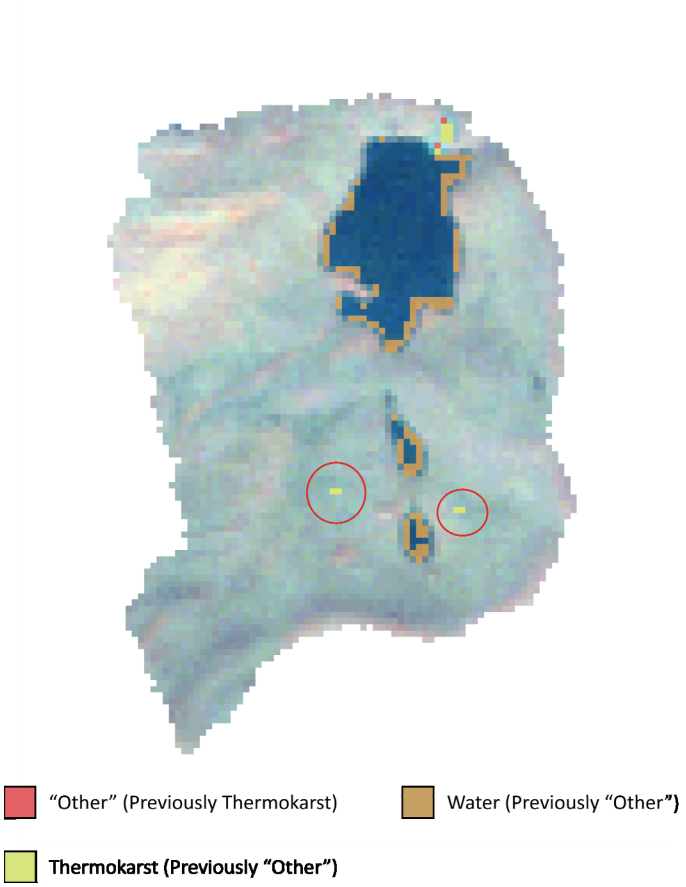

Figure 4.4. SPOT-Landsat change detection.

The third trial performed involved a CIR-Landsat change detection, utilizing the 2006 Landsat image. As already stated, visual inspection of the CIR aerial photograph showed no thermokarst activity, while the 2006 Landsat showed thermokarst activity on the northeast section of the lake.

The results show similarities those found in the other two trials. The model was able detect new areas of thermokarst, but it also identified non-thermokarst areas as thermokarst 36% (0.36 ha out of 0.99 ha of identified thermokarst) of the time. The

model once again had difficulties determining the perimeters of the lakes. In this model; however, the northern section of the lake showed a decrease in the amount of water, while the southern and the eastern portion of Lake 120 showed increases in the amount of water (Figure 4.5). This, like the errors in other models, could be due to rectification errors, errors in spectral ranges, or resampling errors.

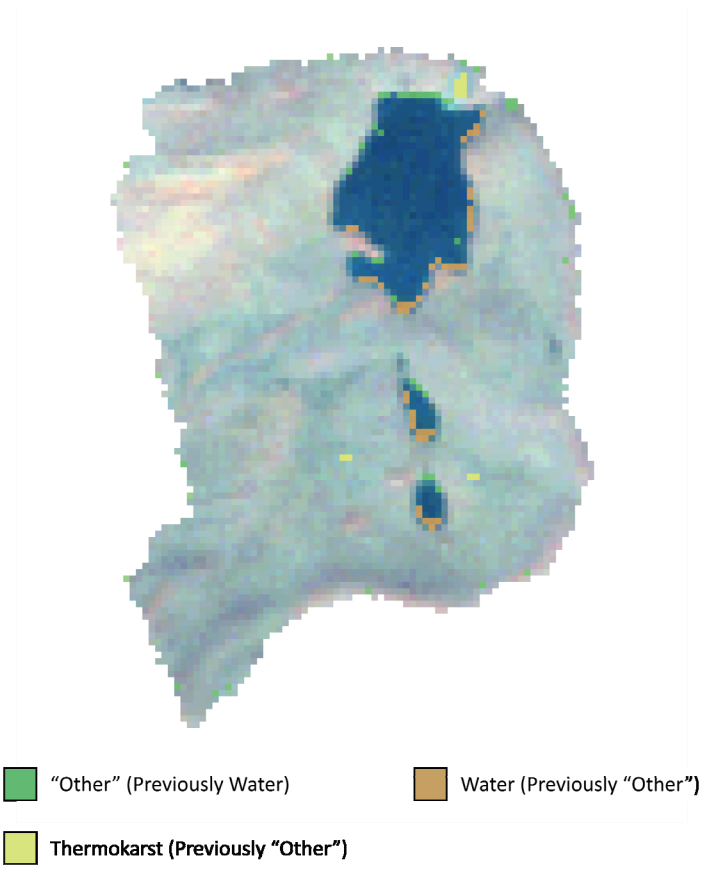

Figure 4.5. CIR-Landsat change detection displayed on the Landsat image.

The final trial was the 2002 Landsat- 2006 Landsat change detection. Visual inspection shows little change in thermokarst activity between the years of 2002 and 2006, except for a little growth in the thermokarst activity on the northeastern shore portion of the lake. The results of the model indicated the growth of the thermokarst activity (0.45 ha (50%) of total model-identified activity), as well as some extraneous thermokarst activity (0.45 ha). Additionally, the model also had issues with indicating extraneous changes in the lake perimeters. This, however, was probably due to resampling that occurred when the 2002 image was projected to match the 2006 image (Figure 4.6).

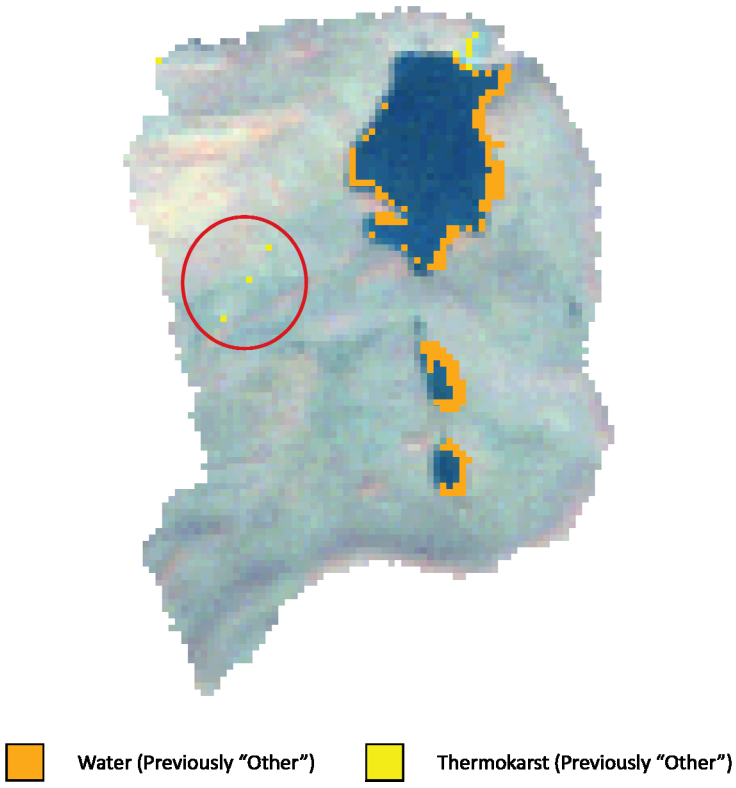

Figure 4.6. Landsat-Landsat change detection.

Campsite Lake Watershed

The first trial was the CIR-SPOT change detection. Visual interpretation of the 1978 CIR aerial photograph showed no evidence of thermokarst activity; however, the 2005 SPOT image showed two appendages on Campsite Lake. One appendage was on the southern shore of the lake, while the second was on the eastern shore of the lake. This might be difficult to pick up with the known perimeter issues the model has with lakes, but because these areas included a large amount of changed pixels concentrated in those areas, it is an indication that those areas should be further investigated (Figure

4.7). The thermokarst activity at Campsite Lake totaled approximately 1.78 ha, and the program was able to extract 1.35 ha (75.8%). Also, the presence of clouds in the 2005 imagery did present extraneous changes (23.6 ha out of 109.97 ha) within the lake in the change detection output (Figure 4.8).

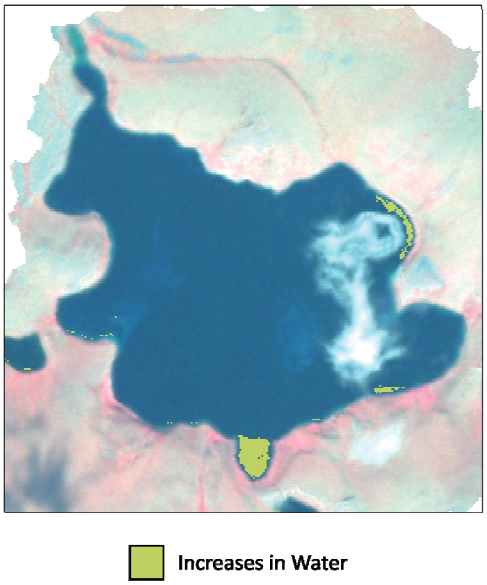

Figure 4.7. Increase in water area at Campsite Lake.

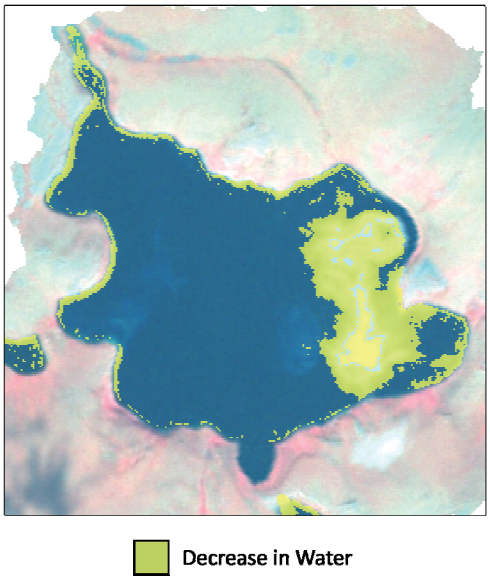

Figure 4.8. Decrease in water category showing a cloud incorrectly as a decrease in water.

The second trial was the SPOT-Landsat change detection model. Visual inspection of the 2005 indicated the presence of the two areas of thermokarst activity, but the 2006 Landsat image did not contain evidence of the thermokarst activity on the southern shore of Campsite Lake. The results of the model indicated the loss of water where the 2005 thermokarst event was previously. When the SPOT image was resampled to a 30-meter X 30-meter resolution, it only showed the loss of a few pixels due to the generalization of pixel values that occurs as a result of resampling. When the original 5-meter X 5-meter resolution SPOT image was used as the before image with the original Landsat image as the after image (30-meter X 30-meter), the loss of the 2005 thermokarst events became more apparent (Figure 4.9). As was true with the

other models, this model showed extraneous change in the water category. The model incorrectly accounted for 34.27 ha of change in the water class.

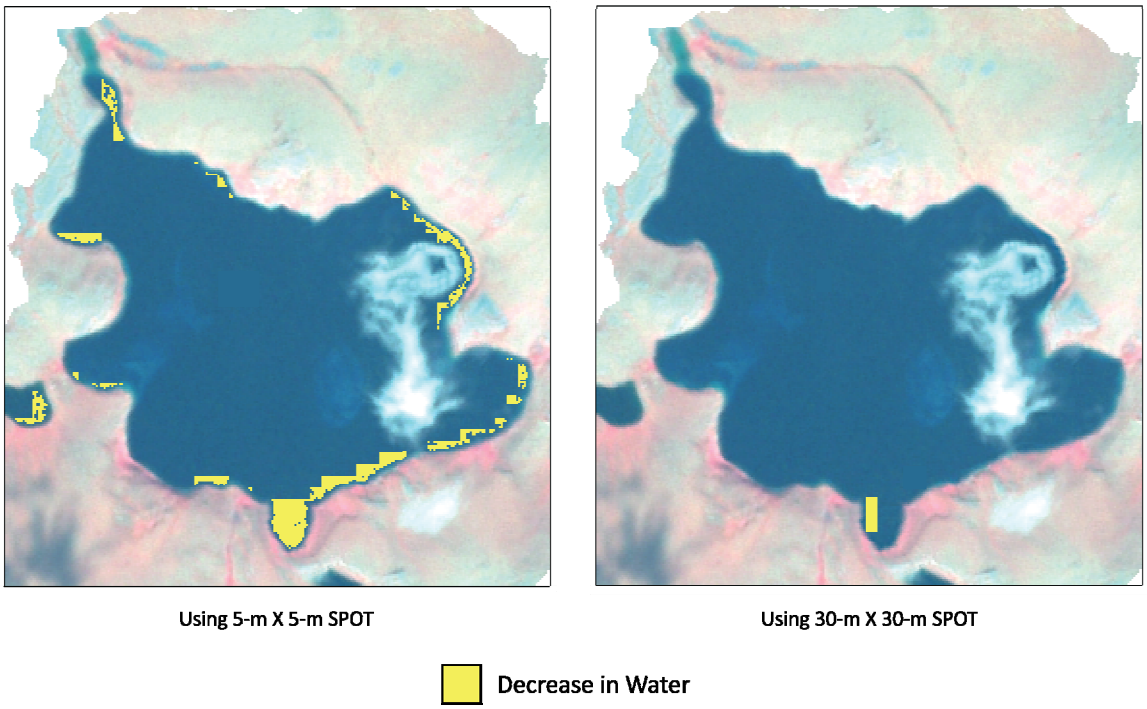

Figure 4.9. SPOT-Landsat change detection showing the decrease in water between 2005 and 2006 using 2 different resolution SPOT images.

The CIR-Landsat and Landsat-Landsat change detection models showed interesting results for this watershed. Between 1978 and 2005, there was a thermokarst event that added area to Campsite Lake; however, in the 2002 and 2006 Landsat image, this area was no longer present on the imagery. As such, the results of both the 1978 CIR aerial photograph and 2006 Landsat change detection and the 2002 and 2006 Landsat change detection both showed no indication of thermokarst activity in

this watershed, only the increases and decreases of water resulting from resampling errors. This indicates the importance for having several years of imagery for an area, because without the 2005 SPOT image, this thermokarst activity at Campsite Lake would have been difficult to locate with satellite imagery, as the CIR-Landsat change detection did not extract any areas of thermokarst activity (Figure 4.10).

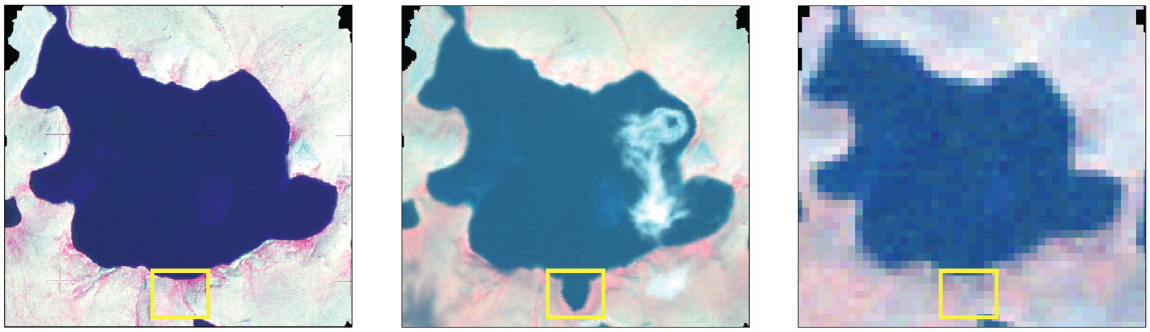

Figure 4.10. Three Campsite Lake images (1978 CIR, 2005 SPOT, 2006 Landsat), in succession, showing the "disappearance" of the thermokarst area.

NE14 Watershed

The NE14 Watershed also has known thermokarst activity, so the same four trials were run. The first trial was the CIR-SPOT change detection. Visual inspection of the 1978 CIR aerial image shows little evidence of thermokarst activity; however, a small lake was present in the northeast section of the watershed, which may be connected to thermokarst activity. In the 2005 SPOT image, a thermokarst area developed where the lake in the northeast section of the watershed was. This thermokarst activity manifests as a barren-like area, connecting to NE14 Lake. The CIR-SPOT model was able to detect

the thermokarst activity in the northeast section of the watershed. Additionally, it detected that a small, .08-ha lake in the northeast section of the watershed was converted to thermokarst activity in the 2005 SPOT image (Figure 4.11). The total area for the thermokarst event present on the 2005 SPOT image was 0.3223 ha. Of that 0.3223-ha area, the program successfully identified 0.165 ha (51.2%). Like in the other watersheds, the model had difficulty extracting the perimeter of the lakes, which could be a combination of any of the issues discussed earlier. Additionally, the model also had difficulty extracting the shallow areas of the lakes (Figure 4.12). Even with these issues, the model only incorrectly identified 3.88 ha (15.3%) of the total water in the watershed (25.42 ha).

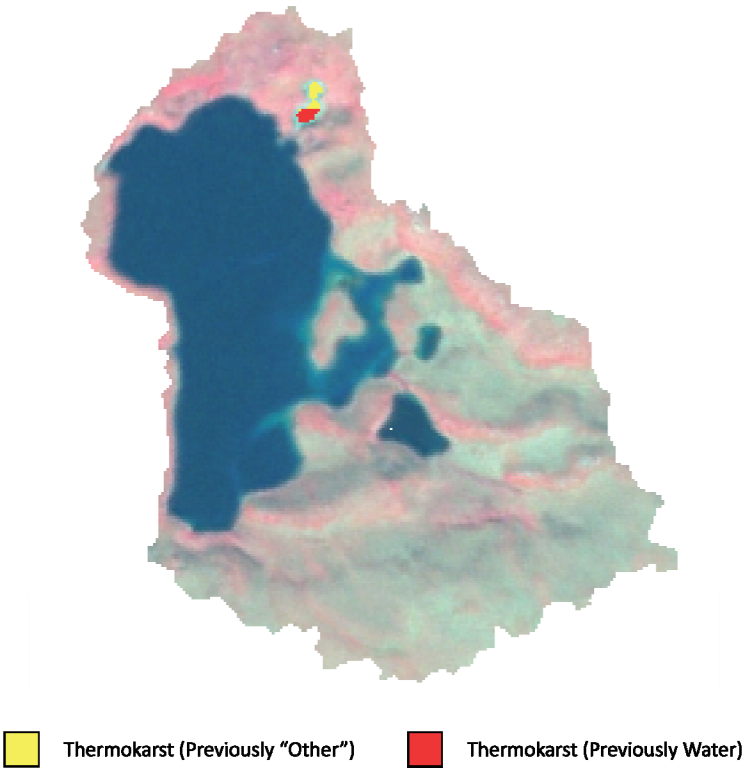

Figure 4.11. Thermokarst detected by the CIR-SPOT change detection model.

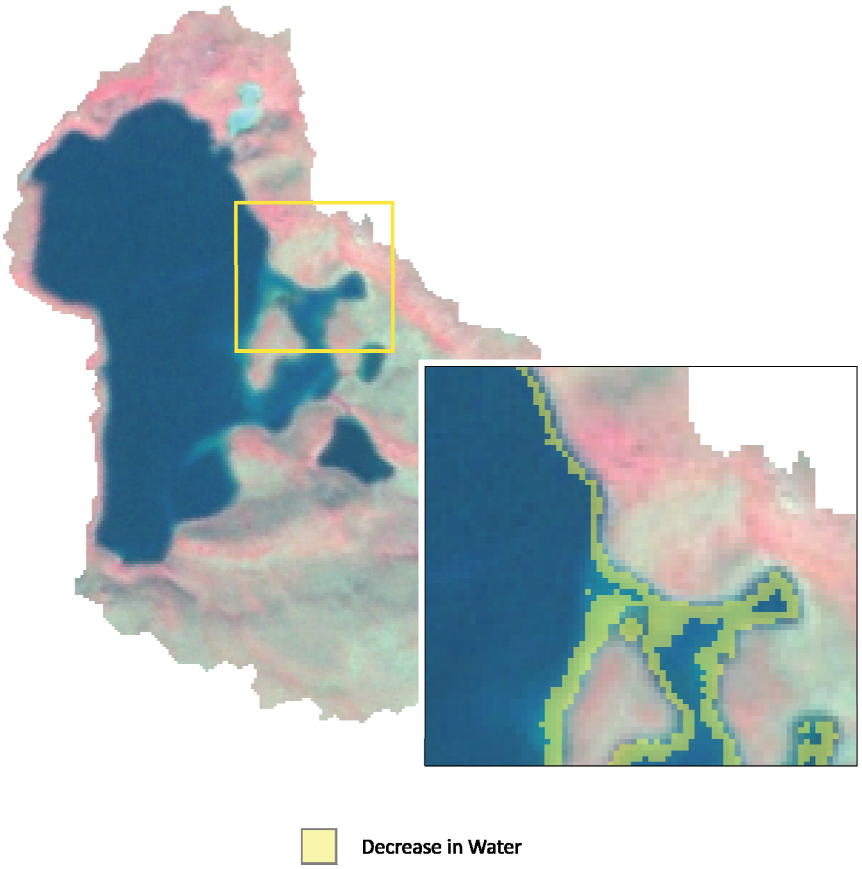

Figure 4.12. Shallow area of water detected as a decrease in water.

The second trial was the SPOT-Landsat change detection. Visual inspection of the 2005 SPOT image showed the thermokarst area on the northeastern shore of NE14 Lake. The 2006 Landsat also contained this area of thermokarst activity; however, it was slightly larger than that of the 2005 SPOT image. Additionally, due to the fact that the SPOT image already contained thermokarst activity, this change detection only detected if those areas became larger. The model was able to determine that the thermokarst that developed between 1978 and 2005 increased in sized, with the change detection showing a value of "3" around the existing thermokarst. The model did however

incorrectly show a pixel in the northwest corner as new thermokarst activity (Figure 4.13). The SPOT-Landsat model was able to correctly identify 0.18 ha of the 0.4 (45%) change in thermokarst activity between the years of 2005 and 2006. The CIR-Landsat change detection shows the same results as the CIR-SPOT and SPOT-Landsat change detections. Out of a 0.87 ha thermokarst area, the model correctly identified 0.27 ha (31%). All three models correctly determined where there was thermokarst activity in the NE14 watershed.

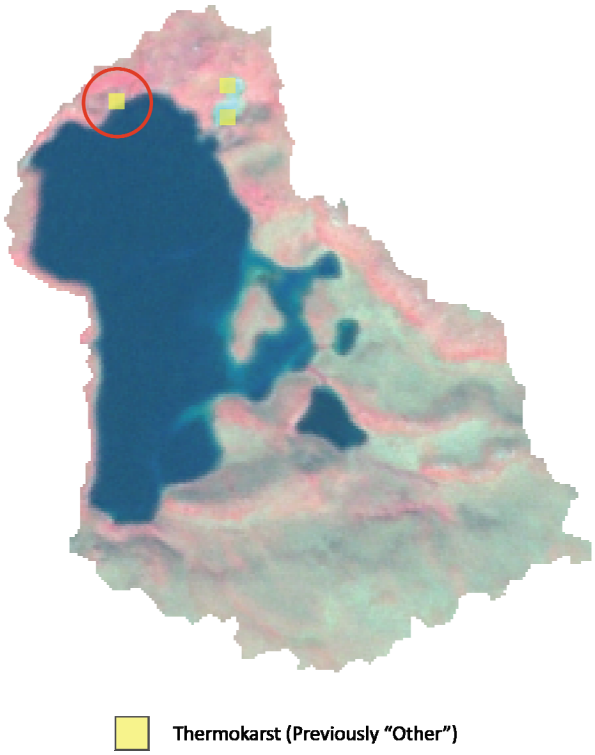

Figure 4.13. Thermokarst activity detected by the SPOT-Landsat change detection model. Potential extraneously detected activity circled in red.

The final trial run on the NE14 watershed was the Landsat-Landsat change detection. Visual inspection of the 2002 Landsat image showed no thermokarst activity present on the image, while the 2006 image showed thermokarst activity along the northeastern shore of Lake NE14. The model was able to identify the thermokarst activity along the northeastern shore. It identified 0.63 ha of the 0.91 ha (69.2%) thermokarst event along the lake's shore, with no extraneous thermokarst activity identified. Figure 4.14 shows this area of thermokarst activity in the northeastern section of the lake as seen in August 2008. This model did, however, have difficulties extracting the lake in the 2006 image. The model showed that the entire lake disappeared, because the spectral values for the lake during that year did not fall into the spectral ranges specified by the model (Figure 4.15).

Figure 4.14. NE14 thermokarst (Photo Credit: Mary Hall-Brown).

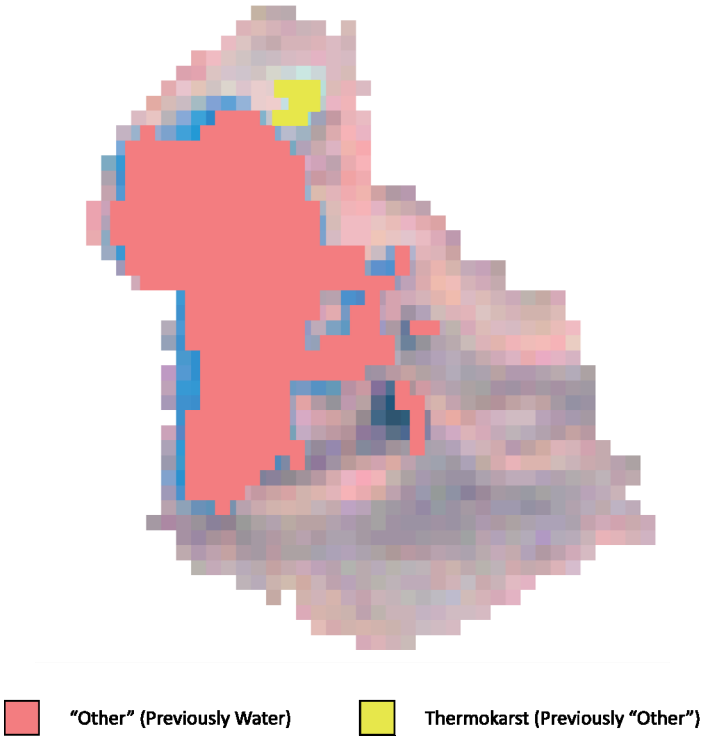

Figure 4.15. Landsat-Landsat change detection for NE14 displayed on the 2006 Landsat image.

4.1.2. Areas without Thermokarst Activity

Lake 100 Watershed

The Lake 100 watershed was chosen to see how well the program performs in areas without known thermokarst activity. As with the other watersheds, three trials were performed to see how well the models responded. Each model, as with the other watershed trials, had difficulty with the perimeters of the lakes; however, no extraneous thermokarst activity was detected within the watershed. The CIR-SPOT model showed 1.05 ha (17.6%) of extraneous water change out of 5.96 ha total water area in the watershed. The SPOT-Landsat model showed 0.9 ha (15.1%) of extraneous water change, and the CIR-Landsat model showed 1.57 ha (26.3%) of extraneous water change. The final trial was the Landsat-Landsat model, which showed 1.98 ha (33.2%) of extraneous water change. This model also, however, showed 0.27 ha of extraneous thermokarst activity (Figure 4.16).

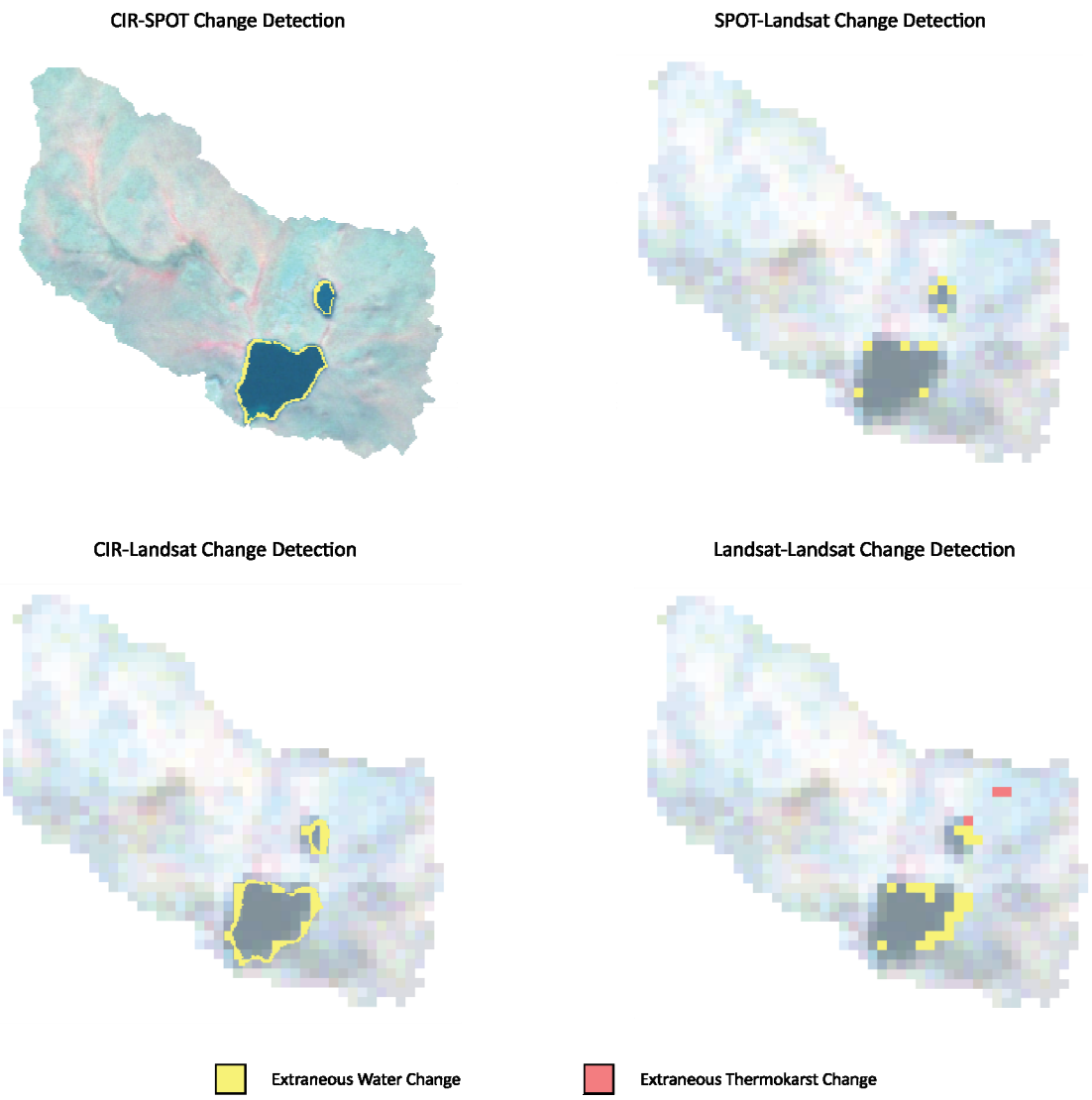

Figure 4.16. Lake 100 watershed change detections.

Island Lake Watershed

The presence of roads and mountains in the Island Lake watershed made it an ideal watershed to test the effectiveness of this program. The first trial was the CIR-SPOT change detection. Visual inspection of both the 1978 CIR aerial photographs and

the 2005 SPOT image revealed no real changes in the lake and no thermokarst activity. The results of the change detection showed extraneous lake changes, as well as the identification of shadows as water (24 ha of extraneous change). Additionally, because the CIR classification model does not have a thermokarst class, parts of the road also were identified as thermokarst activity (5.4 ha). Interestingly, the mountainous areas were not selected as thermokarst activity (Figure 4.17).

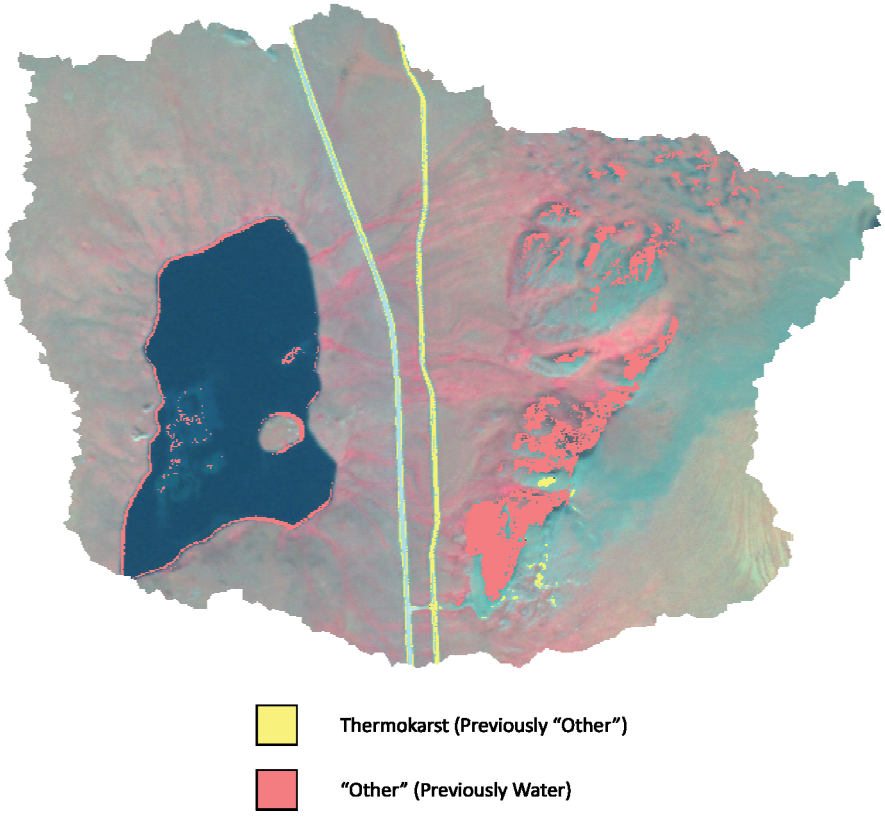

Figure 4.17. Island Lake CIR-SPOT change detection displayed on the SPOT image.

The second trial was the SPOT-Landsat change detection. Just like with the CIR aerial photograph and the SPOT image, no changes in the landscape could be visually seen from the images. In addition to the extraneous lake changes, once again, shadows were identified as extraneous water change (11.25 ha). Also, several mountainous areas were identified as extraneous thermokarst activity (11.61 ha), because they were identified as thermokarst in the Landsat, but not in the SPOT Image (Figure 4.18).

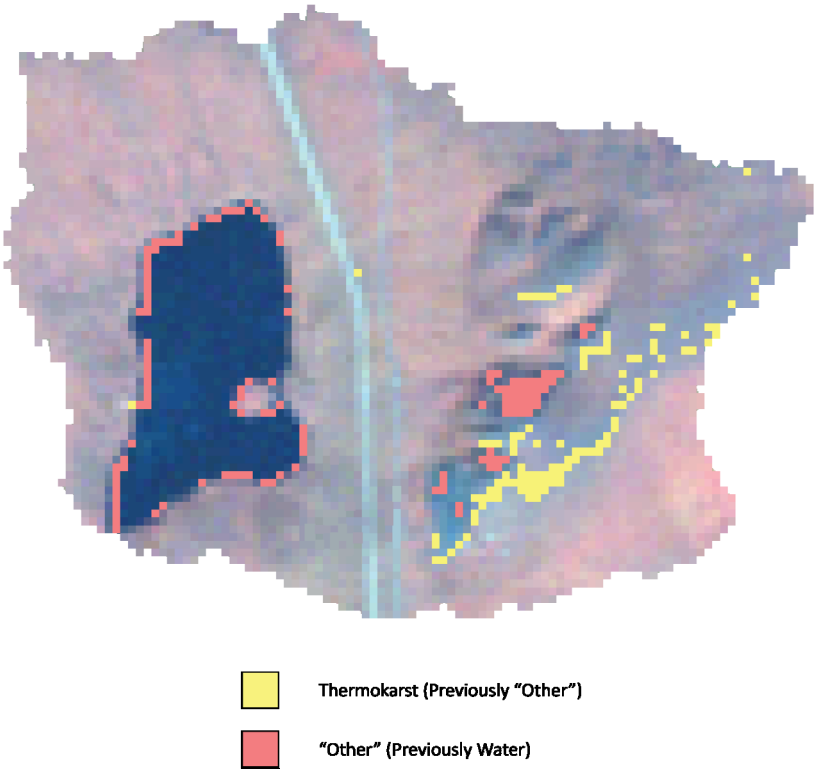

Figure 4.18. Island Lake SPOT-Landsat change detection displayed on the Landsat Image.

The third trial was the CIR-Landsat change detection, which showed similar results to the SPOT-Landsat change detection. Just like in the other images, no visible changes on the landscape were determined prior to running the model. The results indicated 15.84 ha of extraneous water change and 11.88 ha of extraneous thermokarst change in the same areas as the other models. The final model was the Landsat-Landsat change detection trial. Upon visual inspection, there was no difference between the 2002 and 2006 Landsat images for Island Lake; however, the 2002 image did have a shadow in the image. The results of the model were similar to the of the CIR-Landsat and SPOT-Landsat models, showing extraneous water changes of 20.97 ha, including those caused by the shadow in the 2002 image.

NE8 Watershed

The first trial was the CIR-SPOT trial. Visual inspection of the images showed no changes in the lakes that would indicate thermokarst activity. This modeled showed 1.5 ha (out of 28.9 ha total watershed area) of extraneous water change around the perimeter of the lakes (Figure 4.19). The second trial was the SPOT-Landsat change detection model. Like the CIR aerial photograph with the SPOT image, the SPOT and Landsat images showed no indication of thermokarst activity upon visual inspection. Like the CIR-SPOT model, this model only resulted in the identification of extraneous water class changes (2.1 ha) (Figure 4.20). The third trial was the CIR-Landsat change

detection, and the final trial was the Landsat-Landsat change detection. Neither trial showed any changes in the lake in visual inspection or in the model results.

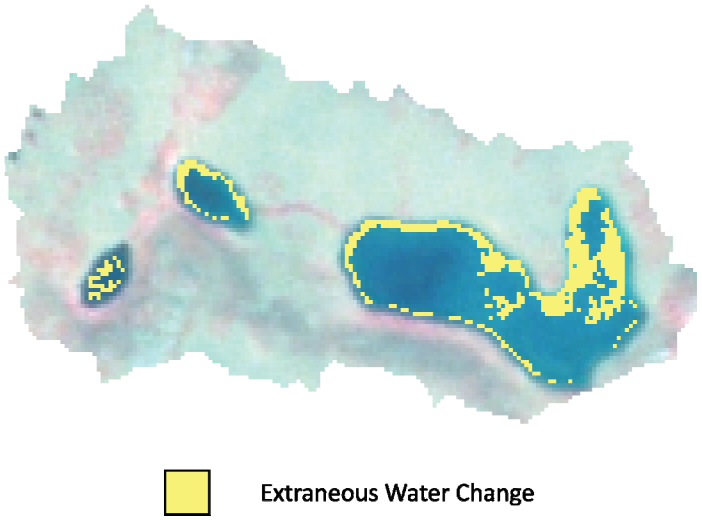

Figure 4.19. NE8 CIR-SPOT change detection displayed on the SPOT image.

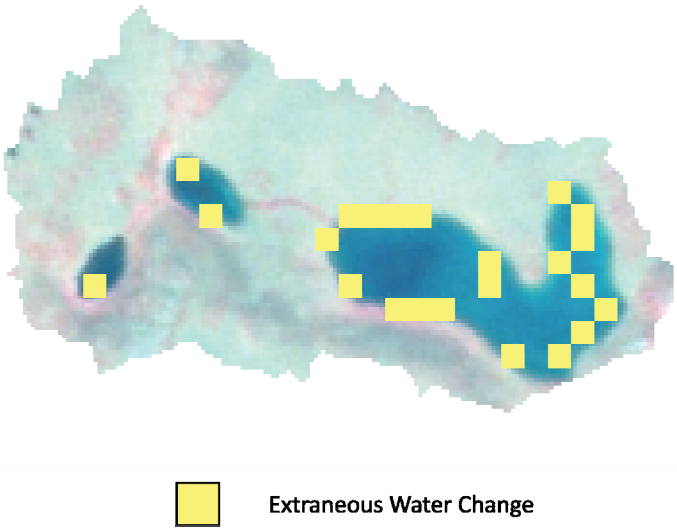

Figure 4.20. NE8 SPOT-Landsat change detection displayed on the SPOT image.

4.2. Summary

Using EML and SML, a program was created within Erdas IMAGINE to automatically extract information about thermokarst activity when two images are input. The program creates two classifications, which are then subtracted from each other to provide a unique number. This unique number provides information as to the phenomena that are occurring in that area of interest, such as the conversion of water to a "thermokarst" area. Though there are inherent problems with providing a range of brightness values to classify imagery, testing of this program proves that it accomplishes its goal of determining areas of potential thermokarst activity.

CHAPTER V

DISCUSSIONS AND CONCLUSIONS

Arctic climate change has been at the forefront of climate change research, because the arctic is considered the most susceptible environment to the effects of global climate change. Additionally, the implications of the effects of climate change in the Arctic have a global scope (Chapin et al. 2005; IPCC 2007; ACIA 2004, Serreze et al. 2000). One indicator and effect of climate change in the Arctic is thermokarst activity. Thermokarst activity in addition to being initiated by climate change, also enhances it, for the activity releases both methane and carbon dioxide (Walter et al. 2006; Hinkel et al. 2005; Osterkamp et al. 2000). Additionally, thermokarst can substantially alter ecosystems or completely convert them to a new ecosystem (Murton 2009; Jorgenson et al. 2001; Osterkamp et al. 2000). Due to the importance of thermokarst in climate change research, it is important to locate these areas of thermokarst activity and research them further.

This research sought to create a program that could determine potential areas of thermokarst activity by automating classification and change detection of various satellite images. Using ERDAS Macro Language (EML) and Spatial Modeling Language (SML), a program and GUI were created to locate several manifestations of thermokarst activity.

Trials on six watersheds in the Alaskan Arctic tested the program's ability to locate and detect these manifestations of thermokarst and other lake changes. Table 5.1 summarizes the thermokarst class results of the trials conducted on those watersheds with known thermokarst activity and those without thermokarst activity. Table 5.2 summarizes the amount of extraneous water changes that resulted from the trials for all six watersheds.

		120	*Campsite*	*NE14*	*100*	*Island Lake*	*NE8*
CIR-SPOT	Correct	0.54 (36%)	1.35 (75.8%)	0.17 (51.2%)	0	0	0
	Incorrect	0	0	0	0	5.4	0
	Identified	0.54	1.35	0.17	0	5.4	0
	Total	1.5	1.78	0.32	0	0	0
SPOT-Landsat	Correct	0.49 (68.1%)	-	0.18 (45%)	0	0	0
	Incorrect	0.49	-	0.09	0	11.61	0
	Identified	0.99	-	0.27	0	11.61	0
	Total	0.72	-	0.4	0	0	0
CIR-Landsat	Correct	0.63 (37.1%)	-	0.27 (31%)	0	0	0
	Incorrect	0.36	-	0	0	11.88	0
	Identified	0.99	-	0.27	0	11.88	0
	Total	1.7	-	0.87	0	0	0
Landsat-Landsat	Correct	0.45 (56%)	-	0.63 (69.2%)	0	0	0
	Incorrect	0.45	-	0	0.27	3.57	0
	Identified	0.9	-	0.63	0.27	3.57	0
	Total	0.8	-	0.91	0	0	0

Table 5.1. Summarization of the results of 120, Campsite Lake, NE14, 100, Island Lake, and NE8 watersheds for the identification of thermokarst change. All values are in hectares (ha).

		120	*Campsite*	*NE14*	*100*	*Island Lake*	*NE8*
CIR-SPOT	Correct	0	0	0	0	0	0
	Incorrect	4.5	23.6	3.8	1.05	24	1.5
	Identified	4.5	23.6	3.8	1.05	24	1.5
	Watershed area	499.86	568.01	78.41	94.26	507.1	28.9
SPOT-Landsat	Correct	0	0	0	0	0	0
	Incorrect	10.4	34.37	5.57	0.9	11.25	2.1
	Identified	10.4	34.37	5.57	0.9	11.25	2.1
	Watershed area	499.86	568.01	78.41	94.26	507.1	28.9
CIR-Landsat	Correct	0	0	0	0	0	0
	Incorrect	8.48	20.25	4.9	1.57	15.84	0.36
	Identified	8.48	20.25	4.9	1.57	15.84	0.36
	Watershed area	499.86	568.01	78.41	94.26	507.1	28.9
Landsat-Landsat	Correct	0	0	0	0	0	0
	Incorrect	13.41	28.62	24.84	1.98	20.97	0
	Identified	13.41	28.62	24.84	1.98	20.97	0
	Watershed area	499.86	568.01	78.41	94.26	507.1	28.9

Table 5.2. Summarization of the results of 120, Campsite Lake, NE14, 100, Island Lake, and NE8 watersheds for the identification of extraneous water change. All values are expressed in hectares (ha), with the "Watershed Area" indicating the total area for that watershed.

The program was able to identify "barren-like" manifestations of thermokarst, appendages on lakes, as well as large losses and gains of water in lakes with moderate success. For the areas of know thermokarst activity, it was able to identify any where from 36 to 81 percent of the activity. The CIR-Landsat model had the highest average percent accuracy (72.5%), which may be due to the 28-year lapse time, potentially yielding larger changes. The program had the highest accuracy in identifying thermokarst as an appendage on an existing lake (Campsite Lake, with an accuracy of

75.8%). All of the models did have problems with the identification of extraneous thermokarst activity when mountains were present (Island Lake watershed results). The identification of extraneous water change activity is another problem with all of the models. Every trial had extraneous water change, which is potentially the result of the resampling that was done to match the spatial resolutions of the various images. There are several potential reasons for this extraneous water change detection. Firstly, natural lake fluctuations could account for the extraneous changes. Also, shallow water areas could indicate areas of change, as they may not fall within the spectral criteria. Also, recall that many of the before images were resampled to match the spatial resolution of the after images. Resampling also changes overall pixel values, and those pixel values may not fall within the spectral ranges. Overall, the program was able to indicate where thermokarst activity is present, even though it may not indicate all of it. As such, the program successfully accomplishes its goal of indicating and identifying thermokarst activity.

One aspect that the program performed very well was in regards to the detection of non-thermokarst areas. Overall the models had an accuracy of 93.8% in the detection of non-thermokarst areas (Table 5.3). If the program can accurately state that certain areas are definitely not thermokarst activity, then these are areas that researchers can eliminate from their potential research. This is especially important when study areas are large.

		100	*Island Lake*	*NE8*
CIR-SPOT	Correct	93.21 (98.9%)	477.6 (94.2%)	27.4 (94.8%)
	Watershed area	94.26	507.1	28.9
SPOT-Landsat	Correct	93.36 (99.1%)	479.1 (94.5%)	26.8 (92.7%)
	Watershed area	94.26	507.1	28.9
CIR-Landsat	Correct	92.69 (98.3%)	478.75 (94.4%)	24.1 (83.4%)
	Watershed area	94.26	507.1	28.9
Landsat-Landsat	Correct	92.28 (97.9%)	461.02 (90.9%)	24.9 (86.3%)
	Watershed area	94.26	507.1	28.9

Table 5.3. Detection of non-thermokarst areas for the no thermokarst watersheds. All areas are in hectares.

Contributions

By successfully completing its objectives, this research has added to the larger body of thermokarst research by allowing researchers to more quickly and efficiently determine thermokarst locations and changes on the landscape. The program created by this research may also reduce manual processing time that is normally required to do a post-classification change detection. The program runs both a "before" classification and an "after" classification, as well as a subtraction of those thematic classifications with the click of one button, and produces an output that provides the user with information on not only what is occurring between the two images but the ability to obtain quantitative "from-to" information. While in some instances not all of the thermokarst area is included in the extraction, it gives the user of the program an indication of where thermokarst activity might be found and what areas need to be more closely investigated. Another advantage of this program is that no preprocessing is required. While it is ideal if the user matches the spatial resolutions of each image, it

is not required. The program will run with imagery of any spatial resolution. Additionally, the program will also run if the image has been degraded or resampled, as long as the sensor input is correct. Finally, the program has been created such that the user can run the program if they have CIR aerial photographs, SPOT images, Landsat images, or any combination of those images. This increases the accessibility and usability of the program by not limiting the users to only one type of imagery, for example using only Landsat.

By reducing manual processing, reducing the preprocessing time necessary, and allowing for multiple image sources, this program successfully reduces the time the user would take to normally identify potential areas of thermokarst activity for further research. This program could also give researchers a general idea of where and how much thermokarst activity is increasing.

Recommendations

Though the program does not require preprocessing to run, it is often best to take into consideration the issues the program has and plan accordingly. For example, the models run by this program have difficulty differentiating the "thermokarst" class from roads, buildings, and mountains. If the imagery utilized by the user has such features, those features could be masked out so that superfluous changes will not be detected. This is especially true if the user wants to run the program in an urban area.

The user might also want to mask out clouds and shadows to also protect from the identification of changes that are not actually present.

Future Research

The program created by this research has flaws in detecting both thermokarst and lake perimeters. Future research should involve spectral refinement of the criteria to more accurately describe these classes and reduce errors of omission and commission. With regards to the difficulty in identifying the perimeters of lakes, lakes may be able to be masked out, so the only activity that will be determined will be the growth or disappearance of a lake. For, if the lake does not appear in one of the two images, it will not be masked out.

The only tests done for the program and its models were within 20 km of the Toolik Lake Research Station in Alaska. This program would also benefit from being tested using imagery in other parts of the Arctic and Subarctic. Additionally, the program would also benefit from being tested in urban areas with known thermokarst activity, such as Fairbanks, Alaska. Testing in urban areas would further widen the use of this program to other applications, such as determining infrastructure responses to urban thermokarst events.

While the program created by this research successfully accomplished its goal, there are several additions that would benefit the program and perhaps aid in a more

successful detection of thermokarst activity. It would be worthwhile to explore adding additional criteria to the model such as slope, normalized difference vegetation index (NDVI), and other parameters to try to rule out some of the pixels that are detected as thermokarst that are known to not be present. As the current program was created based on simplicity and making it available to the widest audience possible in thermokarst research, this would be a new program and models for those researchers who have access to such datasets in addition to imagery brightness values.

REFERENCES

Anisimov, O. A. and Nelson, F. E. (1996). Permafrost and global warming: Strategies of adaptation. In Smith, J. B., Bhatti, N., Menzhuli, G., Benioff, R., Budkyo, M. I., Campos, M., Jallow, B., and Rijsberman, F. (Eds.), *Adapting to climate change* (pp 440 – 449). New York: Springer.

Arctic Climate Change Impact Assessment (2004). *Impacts of a Warming Arctic: Arctic Climate Impact Assessment.* New York: Cambridge University Press.

Armenakis, C. and Savopol, F. (n.d.). Image processing and GIS tools for feature and change extraction. *Natural Resources Canada.*

Balser, A. W., and Walker, D. A. (2003). *Vegetation of the upper Kuparuk River region*. Fairbanks: University of Alaska Fairbanks (Map).

Balser, A. W., and Walker, D. A. (2003). *Landforms of the upper Kuparuk River region*. Fairbanks: University of Alaska Fairbanks (Map).

Burn, C.R. (1992). Canadian Landforms Examples – 24. *The Canadian Geographer, 36*(1): 81-5.

Burn, C.R. (2002). Tundra lakes and permafrost, Richards Island, western Arctic coast, Canada. *Canadian Journal of Earth Sciences, 39*: 1281-1298.

Chapin III, F. S., Sturm, M., Serreze, M. C., McFadden, J. P., Key, J. R., Lloyd, A. H., McGuire, A. D., Rupp, T. S., Lynch, A. H., Schimel, J. P., Beringer, J., Chapman, W. L., Epstein, H. E., Euskirchen, E. S., Hinzman, L. D., Jia, G., Ping, C. L., Tape, K. D., Thompson, C. D. C., Walker, D. A., and Welker, J. M. (2005). Role of land-surface changes in arctic summer warming. *Science, 310*: 657-60.

DeMers, M. N. (2002). *GIS Modeling in Raster*. New York: John Wiley & Sons.

Embleton, C., and King, C.A.M. (1975). *Periglacial Geomorphology*. New York: John Wiley & Sons.

ERDAS (2009). *ERDAS Macro Language: Reference Manual*. Norcross: ERDAS.

Goldman, E. (2002). Even in the high arctic, nothing is permanent. *Science, 297*: 1943-4.

Grosse, G., Schirrmeister, L., Kunitsky, V.V., and Hubberten, H-W. (2005). The use of CORONA images in remote sensing of periglacial geomorphology. An illustration from the NE Siberian coast. *Permafrost and Periglacial Processes, 16*: 163-172.

Hamilton, T.D. (2001). *Glacial geology of Toolik Lake and the upper Kuparuk River region*. Fairbanks: Institute of Arctic Biology.

Harris, S.A. (2002). Causes and consequences of rapid thermokarst development in permafrost or glacial terrain. *Permafrost and Periglacial Processes, 13*: 237-242.

Hinkel, K.M., Frohn, R.C., Nelson, F.E., Eisner, W.R., and Beck, R.A. (2005). Morphometric and spatial analysis of thaw lakes and drained thaw lake basins in the Western Arctic Coastal Plain, Alaska. *Permafrost and Periglacial Processes, 16*: 327-341.

Hinzman, L.D., Bettez, N.D., Bolton, W.R., Chapin, F.S., Dyurgerov, M.B., Fastie, C.L., Griffith, B., Hollister, R.D., Hope, A., Huntington, H.P., Jensen, A.M., Jia, G.J., Jorgenson, T., Kane, D.L., Klein, D.R., Kofinas, G., Lynch, A.H., Lloyd, A.H., McGuire, A.D., Nelson, F.E., Oechel, W.C., Osterkamp, T.E., Racine, C.H., Romanovsky, V.E., Stone, R.S., Stow, D.A., Sturm, M., Tweedie, C.E., Vourlitis, G.L., Walker, M.D., Walker, D.A., Webber, P.J., Welker, J.M., Winker, K.S., and Yoshikawa, K. (2005). Evidence and implications of recent climate change in northern Alaska and other arctic regions. *Climatic Change, 72*: 251-298.

Jensen, J. R. (2005). *Introductory Digital Image Processing: A Remote Sensing Perspective*. 3rd Edition, Upper Saddle River: Prentice-Hall, 525 p.

Jia, G.J. and Epstein, H.E. (2003). Greening of arctic Alaska, 1981-2001. *Geophysical Research Letters, 30*(20): 3-1 – 3-4.

Jorgenson, M.T., Racine, C.H., Walters, J.C., and Osterkamp, T.E. (2001). Permafrost degradation and ecological changes associated with a warming climate in central Alaska. *Climatic Change, 48*: 551-579.

Jorgenson, M.T., Shur, Y.L., and Osterkamp, T.E. (2008). Thermokarst in Alaska. *Ninth International Conference on Permafrost.* Fairbanks.

Kaab, A. (2008). Remote sensing of permafrost-related problems and hazards. *Permafrost and Periglacial Processes, 19*: 107-136.

Kirpotin, S.N., Polishchuk, Y., Bryksina, N. (2009). Abrupt changes of thermokarst lakes in Western Siberia: Impacts of climatic warming on permafrost melting. *International Journal of Environmental Studies, 66*(4): 423-431.

Kodial, P., Toniolo, H., Hinzman, L., and Yoshikawa, K. (2005). Thermokarst evolution in sub-arctic Alaska: A study case. *American Society of Civil Engineers*.

Leica Geosystems Geospatial Imaging (2008). *Leica Geosystems: The IMAGINE Developers' Toolkit*. Norcross: Leica Geosystems Geospatial Imaging.

Mars, J. C., and Houseknecht, D. W. (2007). Quantitative remote sensing study indicates doubling of coastal erosion rate in past 50 yr along a segment of arctic coast of Alaska. *Geology, 35* (7): 583-6.

Murton, J.B. (1996). Thermokarst-lake-basin sediments, Tsktoyaktuk Coastlands, western arctic Canada. *Sedimentology, 43*: 737-760.

Murton, J.B. (2001). Thermokarst sediments and sedimentary structures, Tuktoyaktuk Coastlands, western arctic Canada. *Global and Planetary Change, 28*: 175-192.

Murton, J.B. (2009). Global warming and thermokarst. In R. Margesin (Ed.), *Permafrost Soils* (pp. 185-203). Heidelberg: Spinger.

Osterkamp, T.E., Vierreck, L., Shur, Y., Jorgenson, M.T., Racine, C., Doyle, A., and Boone, R.D. (2000). Observations of thermokarst and its impact on boreal forests in Alaska, U.S.A. *Arctic, Antarctic, and Alpine Research, 32*(3): 303-315.

Osterkamp, T. E. (2005). The recent warming of permafrost in Alaska. *Global and Planetary Change, 49*: 737-60.

Overpeck, J., Hughen, K., Bradley, R., Case, R. Douglas, M., Finney, B., Gajewski, K., Jacoby, G., Jennings, A., Lamoureux, S., Lasca, A., MacDonald, G., Moore, J., Retelle, M., Smith, S., Wolfe, A., Zielinkski, G. (1996). Arctic environmental change of the last four centuries. *Science, 278*: 1251-6.

Rinke, A. and Dethloff, K. (2008). Simulated circum-Arctic climate changes by the end of the 21st century. *Global and Plentary Change. 62*: 173-186.

Romanovsky, V. E., Gruber, S., Jin, H., Marchenko, S. S., Smith, S. L., Trombotto, D., and Walter, K. M. (n.d.) Frozen Ground. 182-200.

Schuur, E. A. G., Crummer, K. G., Vogel, J. G., and Mack, M. C. (2007). Plant species composition and productivity following permafrost thaw and thermokarst in Alaskan tundra. *Ecosystems, 10*: 280-292.

Serreze, M., C., Walsh, J. E., Chapin III, F. S., Osterkamp, T., Dyurgerov, M., Romanovsky, V., Oechel, W. C., Morison, J., Zhang, T., Barry, R. G. (2000). Observational evidence of recent change in the northern high-latitude environment. *Climatic Change, 46*: 159-207.

Smith, L.C., Sheng, Y., MacDonald, G.M., and Hinzman, L.D. (2005). Disappearing arctic lakes. *Science, 308*: 1429.

Solomon, S., Qin, D., Manning, M., Chen, Z., Marquis, M., Averyt, K.B., Tignor, M. and Miller, H.L. (2007). *Contribution of working group I to the Fourth Assessment Report of the Intergovernmental Panel on Climate Change*. New York: Cambridge Press.

Stow, D. A., Hope, A., McGuire, D., Verbyla, D., Gamon, J., Huemmrich, F., Houston, S., Racine, C., Sturm, M., Tape, K., Hinzman, L., Yoshikawa, K., Tweedie, C., Noyle, B., Silapaswan, C., Douglas, D., Griffith, B., Jia, G., Epstein, H., Walker, D., Daeschnre, S., Petersen, A., Zhou, L, and Myneni, R. (2004). Remote sensing of vegetation and land-cover change in arctic tundra ecosystems. *Remote Sensing of the Environment, 89*: 281-301.

Sturm, M., Racine, C., and Tape, K. (2001). Increasing shrub abundance in the arctic. *Nature, 411*: 546-7.

Tanimoto, S.L. (1990). VIVA: A visual language for image processing. *Journal of Visual Languages and Computing, 1*(2): 127-139.

Toniolo, H., Kodial, P., Hinzman, L. D., and Yoshikawa, K. (2008). Spatio-temporal evolution of a thermokarst in Interior Alaska. *Cold Regions Sicence and Technology.*

United States Geological Survey (2010). *Frequently asked questions about the Landsat Missions*. Retrieved from http://landsat.usgs.gov/band_designations_landsat_satellites.php.

Urbach, E. R., and Stepinski, T. F. (2009). Automatic detection of sub-km craters in high resolution planetary images. *Planetary and Space Science, 57*: 880-7.

Vallee, S., and Payette, S. (2007). Collapse of permafrost mounds along a subarctic river over the last 100 years (northern Quebec). *Geomorphology, 90*: 162-170.

Yoshikawa, K. and Hinzman, L. D. (2003). Shrinking thermokarst ponds and groundwater dynamics in discontinous permafrost near Council, Alaska. *Permafrost and Periglacial Processes, 14*: 151-160.

Walker M. D., Walker, D. A., and Auerbach, N. A. (1994). Plant Communities of a tussock tundra landscape in the Brooks Range Foothills, Alaska. *Journal of Vegetation Science, 5* (6): 843-866.

Walker, D. A., Gould W. A., Maier, H. A., and Raynolds, M. K. (2002). The circumpolar arctic vegetation map: AVHRR-derived base maps, environmental controls, and integrated mapping procedures. *Remote Sensing, 23* (21): 4551-70.

Walter, K.M., Zimov, S.A., Chanton, J.P., Verbyla, D., and Chapin III, F.S. (2006). Methane bubbling from Siberian thaw lakes as a positive feedback to climate warming. *Nature, 443*(7): 71-5.

Wolf, B-M. and Heipke, C. (2007). Automatic extraction and delineation of single trees from remote sensing data. *Machine Vision and Applications, 18:* 317-330.

Appendix A: EML code for the GUI and to activate the scripts.

```
component change
{
	variable beforefln;
	variable afterfln;
	variable outputfln;

	frame thermoframe;

	frame thermoframe
	 {
		title "Spectral Thermokarst Detection";
		geometry 0, 0, 500, 450;

		button okb;
		button viewb;
		button cancelb;
		group beforegrp;
			filename beforefln;
			popuplist beforepop;
		group aftergrp;
			filename afterfln;
			popuplist afterpop;
		filename outputfln;

		on framedisplay
		{
			disable okb;
		}


		group beforegrp
		{
			geometry 5,15,243,218;
			filename beforefln
			{
				geometry 36,30,180,3
```

```
                title above left "Before image:";
                select getpref("eml" "default_output_path") + "/*.img";
                filetypedef "raster";
                shortform;
        }

        popuplist beforepop
        {
                geometry 36,120,180,36;
                title above left "Sensor:";
                titlelist
                {
                        "CIR",
                        "SPOT",
                        "Landsat"
                };
                names
                {
                        "CIR",
                        "SPOT",
                        "Landsat"
                };

        }
}

group aftergrp
{
        geometry 252,15,243,218;
        filename afterfln
        {
                geometry 36,30,180,36;
                title above left "After image:";
                select getpref("eml" "default_output_path") + "/*.img";
                filetypedef "raster";
                shortform;
        }

        popuplist afterpop
        {
```

```
                geometry 36,120,180,36;
                title above left "Sensor:";
                titlelist
                {
                        "CIR",
                        "SPOT",
                        "Landsat"
                };
                names
                {
                        "CIR",
                        "SPOT",
                        "Landsat"
                };

        }

}

filename outputfln
{
        geometry 150,270,180,36;
        title above left "Output:";
        select getpref ("eml" "default_output_path")+"/*.img";
        filetypedef "raster" pseudotypes off creatable on;
        newfile;
        shortform;

        on input
        {
                if ($beforefln !="" && $afterfln !="" && $outputfln !="")
                {
                        enable okb;
                }
        }

}


button okb
```

```
{
        title "OK";
        geometry 45,400,90,36;


        on mousedown
        {
                if($beforepop == "CIR" && $afterpop == "Landsat")
                {
                        job modeler -nq "cir-landsat-cd.mdl"
                                quote($beforefln)
                                quote($afterfln)
                                quote($outputfln)
                                -meter
                                -state;
                }
                elsif($beforepop == "CIR" && $afterpop == "CIR")
                {
                        job modeler -nq "cir-cir-cdfin.mdl"
                                quote($beforefln)
                                quote($afterfln)
                                quote($outputfln)
                                -meter
                                -state;
                }
                elsif($beforepop == "CIR" && $afterpop == "SPOT")
                {
                        job modeler -nq "cir-spotcd.mdl"
                                quote($beforefln)
                                quote($afterfln)
                                quote($outputfln)
                                -meter
                                -state;
                }
                elsif($beforepop == "Landsat" && $afterpop == "Landsat")
                {
                        job modeler -nq "landsat-landsat-cd.mdl"
                                quote($beforefln)
                                quote($afterfln)
                                quote($outputfln)
```

```
                    -meter
                    -state;
            }
            elsif($beforepop == "Landsat" && $afterpop == "SPOT")
            {
                job modeler -nq "landsat-spot-cd.mdl"
                    quote($beforefln)
                    quote($afterfln)
                    quote($outputfln)
                    -meter
                    -state;
            }
            elsif($beforepop == "SPOT" && $afterpop == "Landsat")
            {
                job modeler -nq "spot-landsat-cd.mdl"
                    quote($beforefln)
                    quote($afterfln)
                    quote($outputfln)
                    -meter
                    -state;
            }
            elsif($beforepop == "SPOT" && $afterpop == "SPOT")
            {
                job modeler -nq "spot-spot-cd.mdl"
                    quote($beforefln)
                    quote($afterfln)
                    quote($outputfln)
                    -meter
                    -state;
            }
            else unload;
            unload;

        }

}

button viewb
{
        title "View";
```

```
                geometry 208,400,90,36;
                on mousedown
                {
                        modelmaker -open "C:/Program Files/Leica
Geosystems/Geospatial Imaging 9.2/etc/models/cir-spotcd.gmd";
                }
        }

        button cancelb
        {
                title "Cancel";
                geometry 373,400,90,36;
                on mousedown
                {
                        unload;
                }
        }

}

on startup
{
        display thermoframe;
}


}
```

Appendix B: MDL Scripts for the models.

1. CIR-CIR

```
COMMENT "Generated from graphical model: l:/alaska/geo 613/models and scripts/cir-cir-cd.gmd";
# CIR
# CIR
#
# set cell size for the model
#
SET CELLSIZE MIN;
#
# set window for the model
#
SET WINDOW UNION;
#
# set area of interest for the model
#
SET AOI NONE;
#
# declarations
#
Integer RASTER beforefln FILE OLD NEAREST NEIGHBOR AOI NONE arg1;
Integer RASTER afterfln FILE OLD NEAREST NEIGHBOR AOI NONE arg2;
Integer RASTER outputfln FILE DELETE_IF_EXISTING USEALL ATHEMATIC 8 BIT SIGNED INTEGER arg3;
#
# function definitions
#
#define n8_memory Integer(CONDITIONAL {($afterfln(1)>9 && $afterfln(1)<45 && $afterfln(2)>=0 && $afterfln(2)<74 && $afterfln(3)>36 && $afterfln(3)<117) 1,\
        (DEFAULT) 6})
#define n7_memory Integer(CONDITIONAL {($beforefln(1)>9 && $beforefln(1)<45 && $beforefln(2)>=0 && $beforefln(2)<74 && $beforefln(3)>36 && $beforefln(3)<117) 1,\
        (DEFAULT) 6})
outputfln = $n7_memory - $n8_memory;
QUIT;
```

2. CIR-Landsat

```
COMMENT "Generated from graphical model: l:/alaska/geo 613/models and scripts/cir-landsat-cd.gmd";
# CIR
# LANDSAT
#
# set cell size for the model
#
SET CELLSIZE MIN;
#
# set window for the model
#
SET WINDOW UNION;
#
# set area of interest for the model
#
SET AOI NONE;
#
# declarations
#
Integer RASTER beforefln FILE OLD NEAREST NEIGHBOR AOI NONE arg1;
Integer RASTER afterfln FILE OLD NEAREST NEIGHBOR AOI NONE arg2;
Integer RASTER outputfln FILE DELETE_IF_EXISTING USEALL ATHEMATIC 8 BIT SIGNED INTEGER arg3;
#
# function definitions
#
#define n6_memory Integer(CONDITIONAL {($afterfln(4)>4 && $afterfln(4)<16 && $afterfln(3)>6 && $afterfln(3)<20 && $afterfln(2)>10 && $afterfln(2)<24) 1,\
        ($afterfln(4)>24 && $afterfln(4)<30 && $afterfln(3)>21 && afterfln(3)<30 && $afterfln(2)>17 && $afterfln(2)<25) 3,\
        (DEFAULT) 6})
#define n5_memory Integer(CONDITIONAL {($beforefln(1)>9 && $beforefln(1)<45 && $beforefln(2)>=0 && $beforefln(2)<74 && $beforefln(3)>36 && $beforefln(3)<117) 1,\
        (DEFAULT) 6})
outputfln = $n5_memory - $n6_memory;
QUIT;
```

3. CIR-SPOT Model

```
COMMENT "Generated from graphical model: i:/alaska/geo 613/models and scripts/cir-spotcd.gmd";
# CIR
# SPOT
#
# set cell size for the model
#
SET CELLSIZE MIN;
#
# set window for the model
#
SET WINDOW UNION;
#
# set area of interest for the model
#
SET AOI NONE;
#
# declarations
#
Integer RASTER beforefln FILE OLD NEAREST NEIGHBOR AOI NONE arg1;
Integer RASTER afterfln FILE OLD NEAREST NEIGHBOR AOI NONE arg2;
Integer RASTER outputfln FILE DELETE_IF_EXISTING USEALL ATHEMATIC 8 BIT SIGNED INTEGER arg3;
#
# function definitions
#
#define n6_memory Integer(CONDITIONAL {($afterfln(1)>57 && $afterfln(1)<83 && $afterfln(2)>36 && $afterfln(2)<70 && $afterfln(3)>17 && $afterfln(3)<30) 1,\
        ($afterfln(1)>90 && $afterfln(1)<145 && $afterfln(2)>115 && $afterfln(2)<150 && $afterfln(3)>50 && $afterfln(3)<110) 3,\
        (DEFAULT) 6})
#define n5_memory Integer(CONDITIONAL {($beforefln(1)>9 && $beforefln(1)<45 && $beforefln(2)>=0 && $beforefln(2)<74 && $beforefln(3)>36 && $beforefln(3)<117) 1,\
        (DEFAULT) 6})
outputfln = $n5_memory - $n6_memory;
QUIT;
```

4. Landsat-Landsat Model

```
COMMENT "Generated from graphical model: l:/alaska/geo 613/models and
scripts/landsat-landsat-cd.gmd";
# LANDSAT
# LANDSAT
#
# set cell size for the model
#
SET CELLSIZE MIN;
#
# set window for the model
#
SET WINDOW UNION;
#
# set area of interest for the model
#
SET AOI NONE;
#
# declarations
#
Integer RASTER beforefln FILE OLD NEAREST NEIGHBOR AOI NONE arg1;
Integer RASTER afterfln FILE OLD NEAREST NEIGHBOR AOI NONE arg2;
Integer RASTER outputfln FILE DELETE_IF_EXISTING USEALL ATHEMATIC 8 BIT SIGNED
INTEGER arg3;
#
# function definitions
#
#define n6_memory Integer(CONDITIONAL {($afterfln(4)>4 && $afterfln(4)<16 &&
$afterfln(3)>6 && $afterfln(3)<20 && $afterfln(2)>10 && $afterfln(2)<24) 1,\
        ($afterfln(4)>24 && $afterfln(4)<30 && $afterfln(3)>21 && $afterfln(3)<30 &&
$afterfln(2)>17 && $afterfln(2)<25) 3,\
        (DEFAULT) 6})
#define n5_memory Integer(CONDITIONAL {($beforefln(4)>4 && $beforefln(4)<16 &&
$beforefln(3)>6 && $beforefln(3)<20 && $beforefln(2)>10 && $beforefln(2)<24) 1,\
        ($beforefln(4)>24 && $beforefln(4)<30 && $beforefln(3)>21 &&
$beforefln(3)<30 && $beforefln(2)>17 && $beforefln(2)<24) 3,\
        (DEFAULT) 6})
outputfln = $n5_memory - $n6_memory;
QUIT;
```

5. Landsat-SPOT Model

```
COMMENT "Generated from graphical model: l:/alaska/geo 613/models and
scripts/landsat-spot-cd.gmd";
# LANDSAT
# SPOT
#
# set cell size for the model
#
SET CELLSIZE MIN;
#
# set window for the model
#
SET WINDOW UNION;
#
# set area of interest for the model
#
SET AOI NONE;
#
# declarations
#
Integer RASTER beforefln FILE OLD NEAREST NEIGHBOR AOI NONE arg1;
Integer RASTER afterfln FILE OLD NEAREST NEIGHBOR AOI NONE arg2;
Integer RASTER outputfln FILE DELETE_IF_EXISTING USEALL ATHEMATIC 8 BIT SIGNED
INTEGER arg3;
#
# function definitions
#
#define n6_memory Integer(CONDITIONAL {($afterfln(1)>57 && $afterfln(1)<83 &&
$afterfln(2)>36 && $afterfln(2)<70 && $afterfln(3)>17 && $afterfln(3)<30) 1,\
        ($afterfln(1)>90 && $afterfln(1)<145 && $afterfln(2)>115 && $afterfln(2)<150
&& $afterfln(3)>50 && $afterfln(3)<110) 3,\
        (DEFAULT) 6})
#define n5_memory Integer(CONDITIONAL {($beforefln(4)>4 && $beforefln(4)<16 &&
$beforefln(3)>6 && $beforefln(3)<20 && $beforefln(2)>10 && $beforefln(2)<24) 1,\
        ($beforefln(4)>24 && $beforefln(4)<30 && $beforefln(3)>21 &&
$beforefln(3)<30 && $beforefln(2)>17 && $beforefln(2)<25) 3,\
        (DEFAULT) 6})
outputfln = $n5_memory - $n6_memory;
QUIT;
```

6. SPOT-Landsat Model

```
COMMENT "Generated from graphical model: l:/alaska/geo 613/models and
scripts/spot-landsat-cd.gmd";
# SPOT
# LANDSAT
#
# set cell size for the model
#
SET CELLSIZE MIN;
#
# set window for the model
#
SET WINDOW UNION;
#
# set area of interest for the model
#
SET AOI NONE;
#
# declarations
#
Integer RASTER beforefln FILE OLD NEAREST NEIGHBOR AOI NONE arg1;
Integer RASTER afterfln FILE OLD NEAREST NEIGHBOR AOI NONE arg2;
Integer RASTER outputfln FILE DELETE_IF_EXISTING USEALL ATHEMATIC 8 BIT SIGNED
INTEGER arg3;
#
# function definitions
#
#define n6_memory Integer(CONDITIONAL {($afterfln(4)>4 && $afterfln(4)<16 &&
$afterfln(3)>6 && $afterfln(3)<20 && $afterfln(2)>10 && $afterfln(2)<24) 1,\
        ($afterfln(4)>24 && $afterfln(4)<30 && $afterfln(3)>21 && $afterfln(3)<30 &&
$afterfln(2)>17 && $afterfln(2)<25) 3,\
        (DEFAULT) 6})
#define n5_memory Integer(CONDITIONAL {($beforefln(1)>57 && $beforefln(1)<83 &&
$beforefln(2)>36 && $beforefln(2)<70 && $beforefln(3)>17 && $beforefln(3)<30) 1,\
        ($beforefln(1)>90 && $beforefln(1)<145 && $beforefln(2)>115 &&
$beforefln(2)<150 && $beforefln(3)>50 && $beforefln(3)<110) 3,\
        (DEFAULT) 6})
outputfln = $n5_memory - $n6_memory;
QUIT;
```

7. SPOT-SPOT Model

```
COMMENT "Generated from graphical model: l:/alaska/geo 613/models and
scripts/spot-spot-cd.gmd";
# SPOT
# SPOT
#
# set cell size for the model
#
SET CELLSIZE MIN;
#
# set window for the model
#
SET WINDOW UNION;
#
# set area of interest for the model
#
SET AOI NONE;
#
# declarations
#
Integer RASTER beforefln FILE OLD NEAREST NEIGHBOR AOI NONE arg1;
Integer RASTER afterfln FILE OLD NEAREST NEIGHBOR AOI NONE arg2;
Integer RASTER outputfln FILE DELETE_IF_EXISTING USEALL ATHEMATIC 8 BIT SIGNED
INTEGER arg3;
#
# function definitions
#
#define n6_memory Integer(CONDITIONAL {($afterfln(1)>57 && $afterfln(1)<83 &&
$afterfln(2)>36 && $afterfln(2)<66 && $afterfln(3)>17 && $afterfln(3)<26) 1,\
        ($afterfln(1)>90 && $afterfln(1)<145 && $afterfln(2)>115 && $afterfln(2)<150
&& $afterfln(3)>50 && $afterfln(3)<110) 3,\
        (DEFAULT) 6})
#define n5_memory Integer(CONDITIONAL {($beforefln(1)>57 && $beforefln(1)<83 &&
$beforefln(2)>36 && $beforefln(2)<70 && $beforefln(3)>17 && $beforefln(3)<30) 1,\
        ($beforefln(1)>90 && $beforefln(1)<145 && $beforefln(2)>115 &&
$beforefln(2)<150 && $beforefln(3)>50 && $beforefln(3)<110) 3,\
        (DEFAULT) 6})
outputfln = $n5_memory - $n6_memory;
QUIT;
```